



Contents lists available at ScienceDirect

## Materials Science & Engineering B

journal homepage: [www.elsevier.com/locate/mseb](http://www.elsevier.com/locate/mseb)



### Highlights

#### A test of meta-heuristic algorithms for parameter extraction of next-generation solar cells with S-shaped current-voltage curves

Oleg Olikh

- 14 meta-heuristic algorithms are used to parameter estimation from S-shaped *IV* curves.
- The algorithms' efficiencies are compared by using nonparametric statistic methods.
- The relevance of using the square error fitness function has been demonstrated.
- STLBO and ADELI excel in identifying parameters of the opposed two-diode model.

Materials Science & Engineering B xxx (xxxx) xxx

**Graphical abstract and Research highlights will be displayed in online search result lists, the online contents list and the online article, but will not appear in the article PDF file or print unless it is mentioned in the journal specific style requirement. They are displayed in the proof pdf for review purpose only.**



# A test of meta-heuristic algorithms for parameter extraction of next-generation solar cells with S-shaped current–voltage curves

Oleg Olikh

Taras Shevchenko National University of Kyiv, 64/13, Volodymyrska Street, Kyiv, 01601, Ukraine

## ARTICLE INFO

**Keywords:**

S-shaped IV characteristics  
Opposed two-diode model  
Parameter estimation  
Meta-heuristic algorithms  
Nonparametric statistical procedure  
Solar cell models

## ABSTRACT

Identifying parameters of photovoltaic (PV) models based on measured current–voltage (*IV*) characteristic curves is critical for simulating, evaluating, and controlling PV systems. *IV* characteristics of the latest-generation solar cells (SCs) often display an S-shaped deformation. In this paper, we explore the potential of meta-heuristic algorithms to address the parameter estimation problems associated with PV cells that exhibit S-shaped *IV* characteristics. This estimation is performed within the framework of the opposed two-diode model. We implemented a total of 14 algorithms from various classes to extract the SC parameters from synthetic *IV* curves, which were generated using a range of parameter values. The results were compared by using nonparametric statistical methods. These methods include the Wilcoxon signed-rank test for pairwise comparisons, and the Friedman, Friedman Aligned, and Quade tests for multiple comparisons. Comprehensive results and analyses show that the STLBO (Simplified teaching–learning based optimization algorithm) and ADELI (Adaptive differential evolution with the Lagrange interpolation argument) algorithms demonstrate highly competitive performance in terms of accuracy and reliability. This paper underscores the efficacy of advanced meta-heuristic algorithms in solving complex non-linear optimization problems in the domain of photovoltaic research, particularly concerning the unique challenges posed by S-shaped *IV* characteristics of new-generation solar cells.

## 1. Introduction

The intensive use of fossil fuels has led to numerous ecological and energy-related challenges for humanity. Addressing these issues, the most hopeful solution appears to be the adoption of renewable green energy sources. However, this requires tackling several key tasks, the primary among them being the direct generation of energy and the ability to store it to ensure a reliable supply. Whereas the latter can be addressed through the development of energy storage devices (such as lithium-ion batteries or next-generation dual-ion batteries [1–3]), photovoltaics (PV) is widely regarded as the most promising clean technology for energy-producing to meet the escalating energy demands of Earth's population. According to the International Energy Agency reports, the cumulative installed PV capacity was forecasted to rise to 1.826 TW by 2026 and 14.5 TW by 2050 [4].

One of the most common approaches to understanding the electrical characteristics of PV devices is the use of an equivalent circuit model. Such lumped-parameter modeling enables simulation, analysis, and optimization of device performance. Currently, silicon solar cells (Si-SCs) comprise approximately 90% of the global PV production capacity. For describing the operation of these conventional SCs, the following

models are most widely utilized: single-diode model (SDM), double-diode model (DDM), and three-diode model (TDM). These models incorporate parallel-connected diodes that activate unidirectionally, a photo-current source, a parallel shunt resistance, and a series resistance. The PV module model (PVMM) is based on the SDM and consists of multiple diodes connected in series and/or parallel. In addition to developing these models, identifying the relevant parameters from current–voltage (*IV*) characteristics is a crucial task.

One prevalent approach for addressing such issues is the utilization of meta-heuristic algorithms. Numerous studies have been undertaken to compare the efficiency of meta-heuristic algorithms for parameter estimation under conventional SC models. Some research studies have focused on a single model, such as SDM [5], DDM [6,7], or TDM [8], while others have examined both SDM and DDM simultaneously [9–12]. Additionally, several publications have investigated the efficiency of algorithms in processing *IV* curves according to three different models: SDM, DDM, and PVMM [13–16], or SDM, DDM, and TDM [17]. A comprehensive survey of meta-heuristic algorithms used for parameter extraction of conventional PV models can be found in the literature [18,19]. Furthermore, the use of conventional SC models

E-mail address: [olegolikh@knu.ua](mailto:olegolikh@knu.ua).

for testing newly developed algorithms is one of the most common approaches, following the utilization of benchmark functions from the Congress on Evolutionary Computation. The diversity of algorithms employed in analyzing conventional models is linked to the No Free Lunch (NFL) theorem [20]. NFL theorem states that no single algorithm can solve all optimization tasks effectively. Consequently, each problem, including the parameter estimation for every equivalent model, requires the selection of a distinct algorithm.

Recently, there has been intensive research focused on innovative developments, further experiments, and practical PV applications of various new-generation solar cells (NG-SCs). The operating principle of NG-SCs is qualitatively similar to that of Si-SCs, but the fourth quadrant of their *IV* characteristics often exhibits an S-shaped kink. The origin of the kink has been attributed to various physical phenomena, and this *IV* characteristics feature is typical among the most promising candidates for NG-SCs. Specifically, S-shaped *IV* curves have been observed in silicon heterojunction SCs [21], thin-film SCs such as CdTe, Cl(G)S, and amorphous silicon PV devices [21,22], normal and inverted organic SCs [23–25], perovskite SCs [21,26], quantum dot SCs [27,28], as well as in hybrid SCs [29–31]. Unfortunately, the conventional models have failed to describe the S-shaped kink adequately. Consequently, new models have been proposed to provide reasonable explanations for the shape of the *IV* curves from an electrical perspective. However, the NFL theorem suggests that algorithms that have demonstrated exceptional results for silicon solar cell models may not yield the same level of effectiveness for NG-SC models. Thus, the relevant task arises of selecting appropriate meta-heuristic algorithms for extracting parameters from the S-shaped *IV* curves. Certainly, meta-heuristic algorithms have been utilized in processing experimental S-shaped *IV* curves [32]. Nevertheless, to our knowledge, studies aimed at identifying the most optimal approach for solving these problems are currently lacking.

This study aimed to compare the effectiveness of meta-heuristic algorithms in extracting the parameters of NG-SCs from the S-shaped *IV* curves and to determine the most suitable ones for addressing this optimization problem. The parameters extraction has been done according to the De Castro two-diode model based on synthetic *IV* characteristics. The peculiarities of the De Castro model compared to others proposed for describing S-shaped curves, as well as the rationale for its selection, are detailed in Section 2.1. Section 2.2 deals with the procedure for generating synthetic *IV* curves. The investigation focused on 14 metaheuristic algorithms, briefly outlined in Section 2.3. Some of these algorithms have been well-known for a long time and have proven their effectiveness in solving a wide range of problems. Other algorithms are more recent and have been developed using the knowledge gained from their predecessors. When comparing the efficiency of algorithms, considerations were taken into account for computation speed, accuracy of parameter determination, and result repeatability. The comparison was carried out using various nonparametric statistical methods. The specific comparison criteria and nonparametric methods utilized are detailed in Section 2.4. The results of both pairwise and multiple comparisons are detailed in Section 3. Finally, we conclude this paper in Section 4.

## 2. Problem definition

### 2.1. Opposed two-diode model

Today, a considerable number of models have been proposed with the aim of explaining S-shaped *IV* curves. One of the earliest attempts was proposed by Mazhari [33]. This model is essentially a simplified version of the SDM, achieved by excluding resistances and incorporating an additional diode. But Mazhari's model fails to capture the linear-like rise of the S-shaped kink in the third quadrant. An improved model, which incorporates two resistances, was proposed for organic SCs [34]. Gaur and Kumar [23] offered equivalent model to represent the behavior of polymer SC in the dark. This model is almost identical

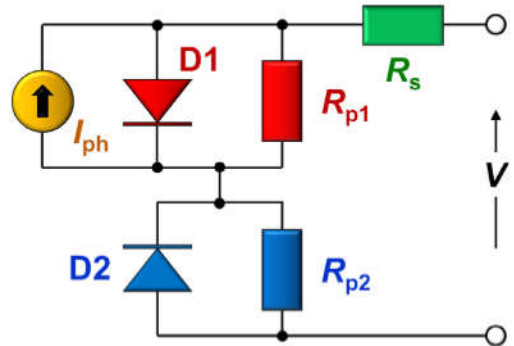


Fig. 1. The opposed two-diode equivalent-circuit model of a solar cell [36].

to the DDM, except that one of the diodes has the opposite polarity. Another approach to developing equivalent models involves using multiple series-connected diodes. Zuo et al. [35] proposed a model consisting of two series-connected diodes in the same direction, two shunt resistors, and one series resistor. Another equivalent circuit holds two opposed diodes, two opposed current sources, and no resistors [27]. De Castro et al. [36] proposed a model consisting of two opposed diodes with shunt resistance for each, a series resistance, and a photo-current source — see Fig. 1. Further modifications to this model include adding a third diode that would either replace one of the shunt resistances [37] or be placed in parallel [22,38]. In general, the development of models to describe S-shaped *IV* curves continues. For instance, a relatively recent proposal is the B2BDM model [39]. This model includes back-to-back diodes parallel with a shunt resistor and the photo-current source, all in series with an offset voltage source. This assembly is then connected in parallel to another diode and shunt resistor, again in series with a resistor. Some review about models for PV devices with S-shaped *IV* curves can be found in [40,41].

Our study focused on the opposed two-diode model, proposed by De Castro [36]. This model represents a significant advancement as it successfully reproduces the S-shaped kink in the power-producing fourth quadrant of the illuminated *IV* characteristics. However, it encounters difficulties in accurately describing the *IV* curve beyond the open-circuit point in the first quadrant. Despite this drawback, the model is gaining attention for deriving analytical solutions of equivalent circuits [28] and is widely used to describe experimental *IV* curves of SCs with different structures [32,42–49]. In particular, these include polymer [46] and polymer/fullerene [44] bulk heterojunction photovoltaic cells, ternary organic solar cells [47], and other types of organic structures [32,43], perovskite solar cells with fullerene transport layer and carbon nanotube electrode [49], and perovskite solar cells with ionic liquid gating [48]. The popularity of the De Castro model is also because, in experiments, *IV* curves are typically measured only in the fourth quadrant from short-circuit current to open-circuit voltage. Therefore, our selection of the two-diode model is based on its universality and widespread applicability.

It can be seen from the model structure, as shown in Fig. 1, that some elements are identical to SDM. It is a current source accompanied by a diode D1, a shunt resistor  $R_{p1}$  to represent the leakage current, and a series resistor  $R_s$  to account for the losses associated with the load current. However, SDM fails to describe the S-shaped kink, which requires additional elements. As a result, a second diode (D2) and a second parallel resistor ( $R_{p2}$ ) are used. D2 is placed opposite D1 and represents the effect of traps at the active layer/cathode interface [36].

The analytical solution  $V(I)$  of the opposed two-diode equivalent circuit model is as follows [50,51]:

$$V(I) = IR_s + \frac{n_1 kT}{q} g(x_1) - \frac{n_2 kT}{q} g(x_2) - \frac{n_1 kT}{q} \ln \left[ \frac{qI_{01}R_{p1}}{n_1 kT} \right] + \frac{n_2 kT}{q} \ln \left[ \frac{qI_{02}R_{p2}}{n_2 kT} \right], \quad (1)$$

with

$$x_1 = \ln \left( \frac{qI_{01}R_{p1}}{n_1kT} \right) + \frac{q(I + I_{ph} + I_{01})R_{p1}}{n_1kT}, \quad x_2 = \ln \left( \frac{qI_{02}R_{p2}}{n_2kT} \right) - \frac{q(I - I_{02})R_{p2}}{n_2kT}, \quad (2)$$

where  $g(x) = \ln(W(\exp(x)))$ ,  $W$  is the Lambert function [52],  $I_{01}$  and  $I_{02}$  are the saturation currents and  $n_1$  and  $n_2$  are the ideality factors for D1 and D2, respectively, and  $I_{ph}$  is the ideal photocurrent. Thus, the model employs eight lumped parameters ( $I_{01}$ ,  $n_1$ ,  $R_{p1}$ ,  $I_{02}$ ,  $n_2$ ,  $R_{p2}$ ,  $R_s$ , and  $I_{ph}$ ) that need to be determined from the IV curve. Thus, from an optimization perspective, the dimension of the problem is  $D = 8$ .

We used Eqs. (1)–(2) for initial simulating IV curves and during the subsequent fitting IV curves procedure with the help of meta-heuristic algorithms. The  $g$ -function was evaluated using an iterative procedure [51].

## 2.2. Synthetic IV curves

The research involved estimating the SC parameters from synthetic IV characteristics simulated using the opposed two-diode model. This approach enables us to assess the accuracy of the optimization meta-heuristic methods used, as the simulation was performed using known parameter values.

In the first part of the study, the performance of meta-heuristic algorithms for parameter estimation was evaluated using a single IV curve. This curve represents the experimental data of bulk heterojunction photocells prepared using a composite of  $p$ -DTS(FBTTh<sub>2</sub>)<sub>2</sub> and neat C<sub>70</sub> [46]. In this case (referred to below as the “Single-IV case”), meta-heuristic algorithms were primarily evaluated through a one-time application. Additionally, the appropriateness of using two different fitness functions was examined. In the second part, we simulated a set of IV characteristics and evaluated the average performance metrics of various algorithms. These curves correspond to the temperature range from 260 K to 350 K. The simulation took into account the temperature dependencies of parameters, closely resembling real SCs. From now on, this case will be referred to as the “IV-set case”. The precise parameter values used in the simulation are listed below.

### 2.2.1. Single-IV case

Previous studies [46,53] have shown that the nonlinear least squares method (NLSM) can be used to fit experimental data from an organic SC, based on the opposed two-diode model, with minimal fitting error. However, the parameter values obtained from the same IV curve with repeated applications of NLSM may differ significantly. Hence, this approach fails to differentiate between similar IV curves derived from SCs with varying parameters.

To overcome this issue, Tada [53] successfully employed Bayesian estimation of parameters. To assess the capabilities of meta-heuristic methods in overcoming similar challenges, they were applied to an IV curve corresponding to such a problematic case. The parameter values were taken from [53]:

$$\begin{aligned} I_{01} &= 1.6 \cdot 10^{-6} \text{ mA}, \quad n_1 = 1.92, \quad R_{p1} = 190 \Omega, \quad I_{02} = 0.16 \text{ mA}, \\ n_2 &= 1.92, \quad R_{p2} = 190 \Omega, \quad R_s = 45 \Omega, \quad I_{ph} = 8 \text{ mA}. \end{aligned} \quad (3)$$

The IV curve was simulated using Eqs. (1)–(2) over a voltage range of 0–0.8 V with a 10 mV step at  $T = 300$  K. The simulation result is presented on Fig. 2 by symbols.

### 2.2.2. IV-set case

Employing various meta-heuristic algorithms to analyze a single IV curve is insufficient for gaining comprehensive insights into the efficacy of these methods in parameter estimation. Furthermore, the accuracy of parameter determination is closely tied to their exact values. For example, an increase in the  $R_p$  value can create challenges in accurately estimating resistance because the shunt will have a reduced impact on

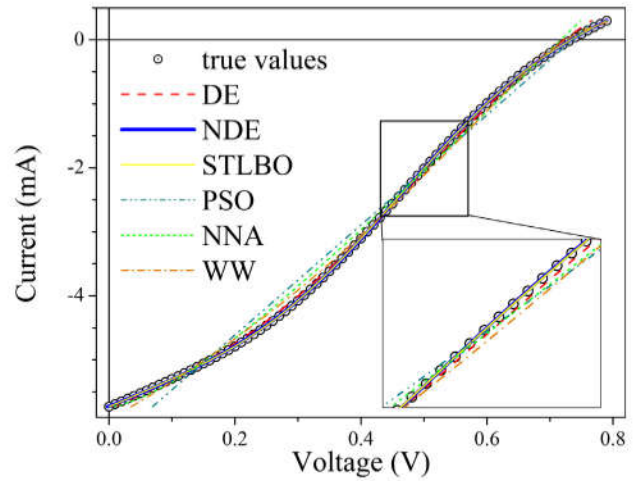


Fig. 2. The current–voltage characteristic is used in the single-IV case (represented by circles). The values from Eq. (3) were assumed during the simulation. Lines display the fitting results of different meta-heuristic algorithms.

the overall shape of the IV curve. Additionally, the ratio between the parameter values is also crucial.

To test the methods across different parameter values, we generated synthetic data within a temperature range of 260 K to 350 K. In the simulation process, we considered the temperature dependencies of the parameters. We based our approach on known physical mechanisms of current flow in NG-SCs and used the reported temperature dependences of saturation current, ideality factor, shunt resistance, and series resistance. However, the main focus was on achieving a diversity of parameter ratios rather than attempting to precisely replicate real-life PV converters of a specific type. Furthermore, an S-shaped IV curve is observed in various types of solar cells, and diverse charge transport mechanisms significantly complicate the selection of a single possible temperature dependence for each of the eight model parameters.

Therefore, we assumed that the current conduction mechanism through D1 is close to tunneling. Hence,  $I_{01}$ ,  $R_{p1}$ , and  $(n_1kT)$  remain constant with the selected values  $I_{01} = 0.015$  mA,  $R_{p1} = 10^4$  Ω,  $n_1kT = 7$  eV. In the case of D2, the thermionic emission current was suggested, and  $I_{02}$  and  $n_2$  increased and decreased, respectively, with rising temperature [54]:

$$I_{02} = I_{002} \exp(-E_I/kT), \quad (4)$$

$$n_2 = 1 + T^*/T, \quad (5)$$

where  $I_{002}$ ,  $E_I$ , and  $T^*$  are the constants which are independent of temperature. The values of  $I_{002} = 500$  A,  $E_I = 0.40$  eV, and  $T^* = 500$  K were used. For  $R_{p2}$ , an exponential temperature dependence was used, as it is commonly observed [55] in NG-SCs for shunt resistance:

$$R_{p2} = R_{p20} \exp(E_R/kT) \quad (6)$$

with  $R_{p20} = 9$  mΩ,  $E_R = 0.32$  eV. The linear temperature dependencies is expected for both  $I_{ph}$  [56,57] and  $R_s$  [58,59]:

$$y = y_0[1 - TC_y(T - 300)], \quad (7)$$

where  $y = I_{ph}$  or  $R_s$ ,  $y_0$  is the parameter value at room temperature,  $TC_y$  is the temperature coefficient of parameter. For most types of monocrystalline silicon solar cells, the  $TC_{I_{ph}}$  typically ranges from around  $-0.0004$  K<sup>-1</sup> [60]. However, as the base thickness decreases, the temperature coefficient can increase to  $-0.0014$  K<sup>-1</sup> [61]. For hydrogenated amorphous silicon solar cells,  $TC_{I_{ph}}$  is equal to  $-10^{-3}$  K<sup>-1</sup> [62]. For organic solar cells, the temperature coefficient can reach a magnitude of  $-0.003$  K<sup>-1</sup> [63]. During the simulation, we assumed  $TC_{I_{ph}} =$

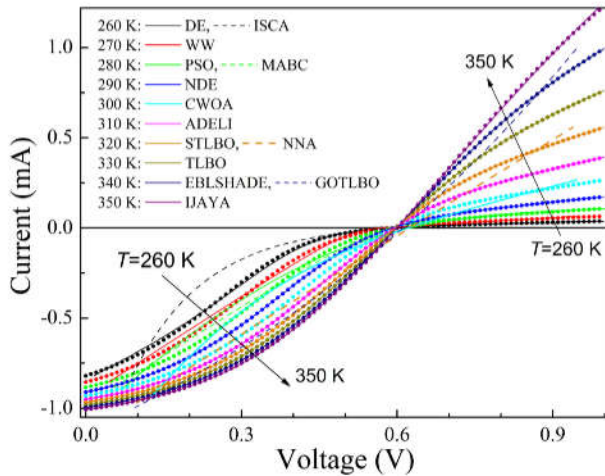


**Fig. 3.** The current–voltage characteristics are used in the IV-set case (represented by symbols). The values from Section 2.2.2 were assumed during the simulation. Lines display the fitting results of different meta-heuristic algorithms.

$-10^{-3} \text{ K}^{-1}$ . Furthermore, the values of  $I_{\text{ph}0} = 1 \text{ mA}$ ,  $\text{TC}_{R_s} = 0.02 \text{ K}^{-1}$ , and  $R_{s0} = 50 \Omega$  were used.

The set of IV data consisted of 10 curves, simulated at 10 K intervals from 260 K to 350 K; in this case,  $n_1$ ,  $I_{02}$ ,  $n_2$ ,  $R_{p2}$ ,  $R_s$ , and  $I_{\text{ph}}$  varied from 6.37 to 4.73, from 9 to 880  $\mu\text{A}$ , from 2.92 to 2.43, from  $1.4 \cdot 10^4$  to 360  $\Omega$ , from 10 to 100  $\Omega$ , and from 0.96 to 1.05 mA, respectively. The IV curves were simulated over a voltage range of 0–1.0 V with a 10 mV step. The simulation results are depicted in Fig. 3 using symbols.

### 2.3. Meta-heuristic algorithms

In the literature, meta-heuristics are frequently categorized based on their sources of inspiration. This categorization involves blending true simulations with stochastic elements to mimic various biological behaviors, natural phenomena, and human behavior characteristics.

On this basis, any meta-heuristic algorithm can fall into one of the following main classes [64–66]: evolution-based methods (emulate the principles of evolutionary behavior observed in creatures in nature by relying on the concept of survival of the fittest), swarm intelligence-based methods (simulate the collective, dynamic, intelligent, and concerted gregarious conduct of collections of flocks or communities found in nature), bio-based methods (use biological processes unrelated to group behavior), chemical & physical-based methods (originate from the physical phenomena or chemical laws that exist in the universe), human-society-based methods (inspired by human beings, including various activities such as thinking and social behavior), and math-based methods (borrow the mathematical functions). Generally, there are hundreds of meta-heuristic optimization methods available. While we acknowledge that our selection may not be fully comprehensive, we utilized 14 methods, representing all classes mentioned above, to tackle the parameter estimation task within the framework of the opposed two-diode model for a solar cell. Hereafter, we will briefly describe each method and the parameters used during the fitting process.

**Differential evolution (DE).** DE is one of the classical methods, and it is based on the natural selection law, utilizing randomly generated initial populations, differential mutation, and probability crossover [67]. We used a penalty function recommended by Ishaque et al. [68] during the implementation process. According to Wang and Ye [67], this work used the following values: mutation scaling factor  $F = 0.8$ , crossover rate  $Cr = 0.3$ , and population size  $Np = 8 \times D = 64$ .

**Adaptive differential evolution with the Lagrange interpolation argument (ADELI).** This improved version of DE incorporates three main elements: local search using Lagrange interpolation, self-adaptive DE

control parameter settings, and an adaptive mutational strategy [69]. The first element involves interpolating three potential solutions using a polynomial function to calculate the local minimum value. The self-adaptive control parameter settings include randomly altering the scaling factor and crossover rate values in each iteration. The adaptive mutational strategy determines the probability of employing Lagrange interpolation in each generation based on the best fitness function value. These incorporations aim to enhance exploitation capability and speed up the convergence. We used parameter values recommended by Huang et al. [69] during the implementation process. Additionally, we set  $Np$  to 64 for our numerical experiments.

**Differential evolution with neighborhood-based adaptive evolution mechanism (NDE).** The method employs a mutation strategy that considers neighborhood and individual information, along with an adaptive evolutionary mechanism [70].  $F$  and  $Cr$  values are determined using a weighted adaptive procedure [71]. The population size is adjusted adaptively using a simple reduction method from  $10 \times D = 80$  to 5.

**Success history based DE with hybridization mutation strategies and population size reduction (EBLSHADE).** The method represents a hybridization framework between the  $p_{\text{best}}$  and  $ord_{p_{\text{best}}}$  mutation strategies. It stores a set of  $Cr$  and  $F$  values that have shown good performance in the recent past [72]. A linear  $Np$  reduction (from  $18 \times D = 144$  to 4) is used as well.

**Particle swarm optimization (PSO).** It is another classic method based on observations of the social behavior of animals, such as bird flocking, fish schooling, and swarm theory. According to Ye et al. [73], the values of learning factors  $l_1 = l_2 = 2$ , the final weight and the initial weight  $w_{\max} = 0.9$ ,  $w_{\min} = 0.4$ , and  $Np = 15 \times D = 120$  are used in this work.

**The modified artificial bee colony (MABC) algorithm.** This algorithm is inspired by the intelligent foraging behavior of honey bee swarms [74]. The control parameters include the population size ( $Np = 8 \times D = 64$ ) and the maximum number of generations, ( $L_{\text{init}} = 36$ ), after which each non-improved food source is discarded.

**Chaotic Whale Optimization Algorithm (CWOA).** Initial algorithm (WOA) draws inspiration from the hunting behavior of humpback whales [75]. Whereas CWOA employs chaotic maps to compute and dynamically adjust its internal parameters [76]. In our study, we utilized the Singer chaotic map and set  $Np = 100$  to identify the SC parameters.

**The neural network algorithm (NNA)** is a meta-heuristic method inspired by both biological nervous systems and artificial neural networks [77]. In our paper, we used the recommended [77] value of  $Np = 50$ .

**The teaching learning based optimization (TLBO) algorithm** utilizes the idea of knowledge transfer within a classroom. Similar to learners acquiring knowledge from a teacher and interacting with their peers, TLBO incorporates these interactions [78]. In this study, a value of  $Np = 100$  is used.

**Generalized oppositional teaching learning based optimization (GOT LBO).** This method utilizes generalized opposition-based learning to enhance basic TLBO through the initialization step and generation jumping, improving convergence speed [79]. The values of jumping rate  $Jr = 1.0$  and  $Np = 20$  were used.

**Simplified teaching–learning based optimization algorithm (STLBO).** In STLBO, the teacher phase is redefined and simplified, while the learner phase remains unchanged [80]. In the redefined teacher phase, the mutation of potential solutions is possible, with the mutation probability decreasing as the iteration number increases. During the early stages, a higher mutation probability helps explore a larger solution space and approach the optimum quickly. However, in the latter stages of optimization, when the teacher (best solution) is near the global optimum, a lower mutation probability serves as a fine-tuning mechanism to enhance local search capability, proving to be an effective strategy. To enrich the mutation behavior, a chaotic sequence is introduced to generate values for the mutation parameters. A chaotic sequence

is a deterministic, random-like process found in nonlinear dynamic systems, which is non-periodic, non-converging, and bounded [81]. Additionally, the elite strategy replaces the worst solutions in the current population with new solutions based on objective function values. The logistic chaotic map and  $N_p = 20$  were used.

**Water wave optimization (WW)** takes inspiration from shallow water wave models and incorporates ideas from wave propagation, refraction, and breaking [82]. WW is easy to implement with a small-size population, and there are four control parameters: the maximum wave height  $h_{max}$ , the wavelength reduction coefficient  $\alpha$ , the breaking coefficient  $\beta$ , and the maximum number  $k_{max}$  of breaking directions. According to Zheng [82], we used the values  $h_{max} = 6$ ,  $\alpha = 1.026$ ,  $N_p = 10$ ,  $k_{max} = \min(12, D/2) = 4$ , and  $\beta$  linearly decreased from 0.25 to 0.001.

**Improved JAYA (IJAYA).** Jaya algorithm is based on the concept that the solution obtained for a given problem should move toward the best solution and should avoid the worst solution and does not require any algorithm-specific parameter [83]. In IJAYA [84], a self-adaptive weight mechanism is introduced to balance the approach towards the optimal solution while simultaneously avoiding the suboptimal solutions. An experience-based learning strategy is utilized to preserve population diversity and enhance exploration capabilities. Additionally, a chaotic elite learning method is proposed to refine the quality of the best solution in each generation. The logistic chaotic map and  $N_p = 4 \times D = 32$  were used.

**Improved sine cosine algorithm (ISCA).** SCA is based on simulating the behaviors of sine and cosine mathematical functions [85]. ISCA implementation included a modified position-updating equation based on inertia weight ( $w_{start} = 1$ ,  $w_{end} = 1$ ), a nonlinear conversion parameter strategy based on the Gaussian function ( $a_{start} = 2$ ,  $a_{end} = 0$ ) [86], the creation of the opposite population to jump out from the local optima with  $Jr = 0.1$  [87], a greedy selection, and  $N_p = 30$ .

The majority of the algorithms used show excellent performance in estimating the SC parameter within conventional models such as SDM or DDM [16, 67, 73, 74, 76, 78–80, 84, 88].

In meta-heuristic optimization methods, the quality of the extracted parameters is evaluated using the fitness function at every iteration. In our investigation, we considered absolute error and square error fitness functions:

$$F_{AE}(Y) = \sum_{k=1}^p |V^{tr}(I_k) - V^{cal}(I_k, Y)|, \quad (8)$$

$$F_{SE}(Y) = \sum_{k=1}^p [V^{tr}(I_k) - V^{cal}(I_k, Y)]^2, \quad (9)$$

where  $V^{tr}(I_k)$  is the simulated value of voltage at current  $I_k$ ,  $V^{cal}(I_k, Y)$  represents the voltage, which is calculated using a set of parameters (i.e.  $Y = \{I_{01}, n_1, R_{p1}, I_{02}, n_2, R_{p2}, R_s, I_{ph}\}$ ) estimated with the help of an algorithm and Eqs. (1)–(2); and  $p$  is the total number of voltage steps in the IV characteristic.

We executed each tested algorithm for  $N_{runs} = 51$  independent runs on every simulated IV curve to generate the statistical results. The search ranges were set as follows:

$$\begin{aligned} I_{01}(\text{mA}) &\in [10^{-13}, 1], n_1 \in [0.5, 50], R_{p1}(\Omega) \in [10, 10^6], I_{02}(\text{mA}) \in \\ &[10^{-7}, 10], n_2 \in [0.5, 50], R_{p2}(\Omega) \in [10, 5 \cdot 10^4], R_s(\Omega) \in [0.1, 1000], \\ &I_{ph}(\text{mA}) \in [10^{-3}, 100]. \end{aligned}$$

#### 2.4. Evaluation metrics

To better illustrate the performance differences between the algorithms being compared, we considered several evaluation metrics. These metrics can be described as follows:

1. Mean value (MEAN), median value (MEDIAN), standard deviance (STD), and interquartile range (IQR) for each two-diode model parameter  $y$  ( $y$  is one of  $\{I_{01}, n_1, R_{p1}, I_{02}, n_2, R_{p2}, R_s, I_{ph}\}$ ). MEAN and MEDIAN are often used to measure the

solution quality. The closer the obtained MEAN and MEDIAN values are to the actual parameter values, the closer the obtained solution is to the optimal solution. To quantify, we used the absolute percentage error (APE):

$$APE(y) = \left| \frac{y - y^{tr}}{y^{tr}} \right|, \quad (10)$$

where  $y^{tr}$  is the parameter value used during the IV curve simulation. APE was calculated for  $y_i$ , obtained by one-run algorithm application ( $APE_i$ ), MEAN ( $APE_{MEAN}$ ), and MEDIAN ( $APE_{MEDIAN}$ ). Reducing STD and IQR result in a more stable algorithm performance.

2. Another criterion for evaluating and comparing algorithm performance is their execution time. We used average run time  $t_{run}$  in seconds for an individual optimizer on one IV curve.
3. The root mean square percentage error (RMSPE) is a statistical measure that indicates how well the fitted curve matches the actual (simulated) IV curve.

$$RMSPE = \sqrt{\frac{1}{p} \sum_{k=1}^p \left[ \frac{V^{tr}(I_k) - V^{cal}(I_k, Y)}{V^{tr}(I_k)} \right]^2}. \quad (11)$$

4. Wilcoxon signed-rank test is a nonparametric statistical test used for pairwise comparisons of algorithms. This test assigns a rank to all the scores considered as one group and then sums the ranks of each group.
5. Friedman, Friedman Aligned, and Quade tests are used for comparing the performance differences among optimization algorithms (multiple comparisons with a control method). Therefore, the average rankings of the algorithms according to the tests are reported. Besides, the post-hoc Finner, Holm, Hochberg, and Holland procedures are used to establish proper comparisons between each algorithm and a set of other algorithms.
6. Multiple Comparisons Test (Friedman) with Shaffer's static, Neemenyi, and Holm procedures are employed to compute all possible pairwise comparisons between groups ( $N \times N$ ) and identify the differences.

Wilcoxon test is used to assess whether there are statistically significant differences between pairs of algorithms. Meanwhile, the Friedman, Friedman Aligned, and Quade tests are employed when it is necessary to compare three or more related groups of results (algorithms). Friedman test evaluates whether there are statistically significant differences between the medians of the ranks of these algorithms. Friedman Aligned Ranks test addresses the issue of rank correlation in the original Friedman test, providing more precise results. Finally, the Quade test helps account for the effects of observed factors, such as random variations, to more accurately determine the statistical differences between groups.

The main drawback of the Friedman, Friedman Aligned, and Quade tests is that they can only detect significant differences over the whole set of multiple comparisons, making it difficult to establish proper comparisons between specific algorithms [89]. To address these issues, it is necessary to employ post-hoc procedures. Post-hoc methods are applied after the initial analysis and allow for controlling the overall error rate when comparing multiple algorithms, thereby reducing the likelihood of randomly identifying statistically significant differences.

$1 \times N$  designs help determine if there are statistically significant differences between one algorithm (the control algorithm) and each of the other algorithms. Multidimensional comparisons  $N \times N$  designs involve analyzing statistical differences between all possible pairs of algorithms. Typically, different post-hoc procedures are used for  $1 \times N$  and  $N \times N$  comparisons. Description of all the used post-hoc procedures can be found in Derrac et al. [89].

All mentioned methods are standard for comparing metaheuristic algorithms [89]. Their comprehensive application enables making the

**Table 1**

The convergence parameters of metaheuristic algorithms in the single-IV case.

Algorithm	$N_{it}$	$N_{FE}$	$t_{run}$ (s)
DE	8000	1 024 000	$42 \pm 1$
EBLSHADE	3000	444 600	$22 \pm 1$
ADELI	12 000	1 800 000	$93 \pm 2$
NDE	5000	430 000	$20.2 \pm 0.3$
MABC	8000	1 024 000	$48 \pm 11$
TLBO	5000	1 000 000	$56.1 \pm 0.3$
GOTLBO	6000	360 000	$15 \pm 1$
STLBO	13 000	273 000	$13.8 \pm 0.3$
PSO	4000	480 000	$19 \pm 3$
IJAYA	30 000	960 000	$37 \pm 1$
ISCA	5000	150 000	$6.5 \pm 0.1$
NNA	5000	250 000	$10.6 \pm 0.5$
CWOA	3000	300 000	$16.6 \pm 0.5$
WW	3000	35 000	$1.4 \pm 0.1$

most well-founded conclusions. As shown below in our case, only applying the entire set of tests and post-hoc methods has enabled us to detect slight differences in the accuracy of model parameter evaluation by different algorithms.

### 3. Numerical results and discussion

#### 3.1. Comparison of algorithm convergence

In meta-heuristic algorithms, various termination conditions can be defined. For instance, a termination condition can be a specific number of iterations  $N_{it}$ , constraints on the number of fitness function evaluations  $N_{FE}$ , a specific rate of precision, a specific time, no sign of change in solutions after a specific number of iterations, or a combination of these cases [90]. In this study, the main focus was on accurately estimating parameters. Therefore, to ensure that both exploration and exploitation processes could be fully realized by each algorithm with an equal opportunity, the termination criterion used was the absence of changes in the solution. Based on this condition, the required number of iterations  $N_{it}$  was determined, and the corresponding calculation time was measured  $t_{run}$ . Figure S1 in the supplementary material shows the convergence curve for the algorithms used. In addition, the  $N_{FE}$  were evaluated.

All the applied algorithms have been coded and implemented in Embarcadero®Delphi 10.3 programming software. The run time was estimated by using WinAPI-functions *QueryPerformanceCounter()* and *QueryPerformanceFrequency()*. The experiments were performed on Windows 10 Pro 64-bit, 2.9 GHz AMD Ryzen 7 4800H CPU, and 8 GB RAM.

The obtained results are listed in **Table 1**. As can be seen from the table, the number of iterations required for an algorithm does not always correlate directly with the number of fitness function evaluations or computation time needed to converge. The reason for this is the unique mathematical operations required by each algorithm. The run time of the algorithms varies considerably, with a range of 1.5 s to 93 s. Notably, WW, ISCA, NNA, and STLBO converge the fastest, while ADELI, TLBO, and MABC require the most time.

#### 3.2. Fitness function selection

To choose the more suitable fitness function, we evaluated each algorithm using the IV curve generated from the parameters provided in Eq. (3) with both  $F_{AE}$  and  $F_{SE}$  functions (see Eqs. (8) and (9)). The results obtained from each of the functions were then compared with each other using pairwise comparisons. The absolute percentage error values obtained for one-run algorithm application ( $APE_i$ ) were used.

**Table 2** gives the statistical results produced by Wilcoxon sign-rank test with a significant level  $\alpha = 0.05$ . The symbol “SE” in a cell indicates that the estimation of the parameter (specified in the column title) by

the algorithm (defined in the first column) with  $F_{SE}$  outperforms the result obtained by this algorithm with  $F_{AE}$ . A cell with “AE” indicates better results for function  $F_{AE}$ . In the case of the symbol “=”, there is no significant difference between function  $F_{SE}$  and function  $F_{AE}$  application.

As evidenced in the provided data, utilizing the square error fitness function more frequently yields better outcomes than  $F_{AE}$ . In some rare cases, the absolute error fitness function can improve the alignment between the fitted and actual curves and enhance the accuracy of parameter estimations by PSO, IJAVA, CWOA, and WW algorithms. However, RMSPE is not the most crucial factor in determining model parameters, and the mentioned methods, as will be shown later, do not provide the highest accuracy. As such, the results presented in the following sections exclusively apply the  $F_{SE}$  function. Therefore, it is recommended that researchers consider the squared error fitness function as a more effective and reliable option for the task of opposed two-diode model parameter estimation.

#### 3.3. Comparison of algorithm performance

##### 3.3.1. Parameter extraction in single-IV case

In this subsection, we present and analyze the statistical results of applying different meta-heuristic algorithms to an IV curve simulated with the values from Eq. (3). Several typical fitting results are shown in **Fig. 2**. A more comprehensive version, including the fitting results obtained using each algorithm, is provided in the supplementary materials (figure S2). It can be seen that the closest match between the approximation curves and the IV curve points is observed for EBL SHADE, ADELI, NDE, IJAYA, TLBO, and STLBO. On the contrary, the fitting curves of PSO and GOTLBO had the least replication of the original data.

**Fig. 4** shows the results of SC parameters estimation by algorithms to be compared. Additionally, the figure presents the RMSPE data, which confirms the conclusions of the visual comparison between the fitting lines and the points of the IV curve. The results for MEAN, MEDIAN, STD, and IQR are presented in table S1 of the supplementary material.

We want to emphasize the following. Firstly, in most cases, median values are more relevant to the actual parameter values than mean values. The only exceptions to this are in the estimation of  $R_s$  and  $R_{p2}$ . However, in cases where a method allows for highly accurate parameter estimation (such as EBL SHADE, ADELI, TLBO, and STLBO), the MEDIANs are at least as good as the MEANS. As a result, we will utilize median values as a robust measure of central tendency in non-parametric statistical tests. Secondly, the increased algorithm stability, as indicated by the reduction in STD and IQR values when determining each model parameter, correlates with improved accuracy in estimating those parameters. Furthermore, IQR values are generally no worse than STD values. Finally, small RMSPE values (a close match between the fitting curve and the IV points) do not always indicate high accuracy in determining the parameters of a solar cell — see IJAYA and NDE data. For example, the difference between the MEDIAN<sub>RMSPE</sub> values for NDE and ADELI is approximately 0.0001 (about 0.08% of their absolute value). However, in the ADELI case, the values of APE<sub>MEDIAN</sub> do not exceed  $6 \cdot 10^{-4}$  for all model parameter estimations. In contrast, when applying the NDE algorithm, the obtained APE<sub>MEDIAN</sub> values are significantly higher, ranging from 0.04 for  $I_{ph}$  to 11.4 for  $I_{01}$ . On the one hand, this confirms the previously mentioned issue identified by Tada [46,53], which arises when estimating parameters according to the opposed two-diode model from similar IV curves corresponding to PV cells with distinct characteristics. Furthermore, the results indicate that some meta-heuristic algorithms, such as NDE and IJAYA, can fall into a similar trap. On the other hand, the high accuracy in parameter estimation demonstrated by EBL SHADE, ADELI, and STLBO indicates that these algorithms can overcome the mentioned issue when applied. It should be noted that a similar problem has been previously addressed

**Table 2**

Wilcoxon signed-rank test results (level of significance  $\alpha = 0.05$ ) for comparing fitness functions. Symbols “SE” and “AE” indicate more precise results obtained using  $F_{\text{SE}}$  and  $F_{\text{AE}}$ , respectively; the symbol “=” suggests no significant difference between the application of functions.

Algorithm	Extracted parameter								RMSPE
	$I_{01}$	$n_1$	$R_{p1}$	$I_{02}$	$n_2$	$R_{p2}$	$R_s$	$I_{ph}$	
DE	SE	SE	=	=	SE	SE	=	=	=
EBLSHADE	SE	=	=	=	=	=	=	=	AE
ADELI	SE	=	=	=	=	=	=	=	AE
NDE	=	=	=	=	=	=	=	SE	SE
MABC	=	SE	=	=	=	=	=	=	SE
TLBO	SE	SE	SE	SE	SE	SE	SE	SE	SE
GOTLBO	=	=	=	=	=	SE	=	=	=
STLBO	SE	=	=	=	=	=	=	=	AE
PSO	=	=	=	=	=	=	AE	=	=
IJAYA	AE	AE	=	=	SE	=	=	=	=
ISCA	=	=	=	=	=	=	=	=	=
NNA	=	=	=	=	=	=	=	=	SE
CWOA	=	=	SE	=	AE	=	=	=	SE
WW	=	=	SE	=	AE	=	=	=	SE

using Bayesian parameter estimation [53]. However, each Bayesian calculation took approximately half a day on a more powerful computer than ours [53]. In contrast, when applying meta-heuristic algorithms in our case, the worst-case run time did not exceed 100 s.

To statistically compare the algorithms under consideration, we used nonparametric tests. In the single-IV case, all nonparametric statistical tests were applied to compare the performance of meta-heuristic algorithms in assessing each of the eight model parameters. APE<sub>i</sub> values were used, and the number of case problems in the study,  $N_{\text{pr}}$ , was equal to  $N_{\text{runs}} = 51$ . Additionally, algorithms were compared in terms of curve-fitting accuracy using RMSPE values. Furthermore, we employed tests for a composite parameter as well. This parameter, referred to as “Comp” hereafter, includes APE<sub>MEDIAN</sub> for each of the eight defined model parameters, the median value for RMSPE, and  $t_{\text{run}}$ . This composite parameter may provide the most valuable insights for comparing the performance of the algorithms. However, it is important to note that the value of  $N_{\text{pr}}$  is only 10. According to Derrac et al. [89], the number of case problems should be  $N_{\text{pr}} \geq 2k$ , where  $k$  is the number of algorithms ( $k = 14$  in our study). Therefore, the use of the Comp parameter is not strictly rigorous. Indeed, it would have been possible to increase the  $N_{\text{pr}}$  value by using, for example, APE<sub>MEAN</sub>. However, deliberately using a suboptimal parameter would have seemed inappropriate.

Fig. 5 graphically depicts the non-parametric statistical results of pairwise comparisons of the algorithms based on the Wilcoxon signed-rank test. For the Comp parameter comparisons, the differences in the performance scores were normalized to the interval [0, 1] to facilitate the comparison. The figure shows that no single algorithm outperforms all the others in evaluating each parameter. Furthermore, no algorithm surpasses all the others when estimating even a single parameter.

For example, as the figure states, STLBO shows a significant improvement over DE, NDE, MABC, GOTLBO, PSO, IJAYA, ISCA, NNA, CWOA, and WW across all the parameters considered with a level of significance  $\alpha = 0.05$ . Simultaneously, no significant differences were detected between the STLBO algorithm and both the EBL SHADE and ADELI algorithms for the estimation of all parameters. Additionally, no significant differences were found between STLBO and TLBO for the Comp parameter comparisons. EBL SHADE outperforms almost all other algorithms in the composite parameter except STLBO. According to the count of victories in the Wilcoxon test, the worst performances are exhibited by PSO and CWOA. PSO achieved better results than ISCA, NNA, and CWOA in RMSPE value and also outperformed WW in  $n_2$  estimation and RMSPE. Test detected significant differences between CWOA and WW in  $n_2$  and  $I_{01}$  estimations, between CWOA and PSO in  $I_{01}$ ,  $I_{02}$ ,  $R_s$ , and  $I_{ph}$  estimations, and between CWOA and both ISCA and NNA in  $R_s$  estimation only.

Looking at the results of the Wilcoxon test from another perspective, it can be observed that neither EBL SHADE nor STLBO suffered any

defeats in pairwise comparisons, while ADELI experienced only one loss. ADELI was defeated in the Comp parameter only by EBL SHADE, primarily due to significantly longer run time. The highest number of defeats was observed for the PSO and WW algorithms (104 and 84, respectively). Fig. 6 summarizes the total number of wins and losses in the Wilcoxon test for each algorithm.

It is recommended [89] to initiate the multiple comparison tests by examining the null hypothesis  $H_0$ , which asserts the equality of medians among the populations of results obtained by different algorithms. The  $p$ -values for the null hypothesis, computed through the statistics of Friedman, Friedman Aligned, and Quade tests and the Iman–Davenport extension, are provided in the supplementary material (table S2). The highest observed  $p(H_0)$ -values were found to be  $2.7 \cdot 10^{-5}$  (Friedman Aligned test for the task of Rp estimation),  $4.4 \cdot 10^{-4}$  (Friedman Aligned test for the composite parameter case), and  $8.3 \cdot 10^{-6}$  (Quade test, Comp parameter). Thus, the obtained data strongly suggest the significant differences among the considered algorithms in the accuracy of all model parameter determination, RMSPE values, and the Comp parameter.

Fig. 7 illustrates the ranks achieved by the Friedman, Friedman Aligned, and Quade tests for the applied optimization algorithms in different tasks. These ranks are also tabulated in the supplementary material (table S3). In nearly all cases, the algorithms EBL SHADE, ADELI, and STLBO consistently achieve the top three ranks. For instance, in assessing the accuracy of model parameter estimation, ADELI has ranked first 22 times. The STLBO algorithm ranked first six times, taking the sole first place twice ( $I_{01}$  estimation according to Friedman Aligned test and  $R_{p1}$  estimation according to Quade test) and sharing it with ADELI four times ( $n_1$ ,  $R_{p1}$ ,  $n_2$ , and  $I_{ph}$  estimation according to Friedman Aligned test). In the RMSPE case, ADELI and STLBO attained equal and top ranks across all three tests utilized. When comparing based on the Comp parameter, the STLBO algorithm secured the top rank according to the Friedman Aligned test, whereas the Friedman and Quade tests identified EBL SHADE as the best performer. For the most part, the TLBO algorithm consistently ranked fourth among all the tested algorithms. Interestingly, in four cases ( $I_{01}$  estimation, RMSPE value, and Comp parameter by Friedman Aligned test, and Comp parameter by Quade test), it even achieved a commendable third-place ranking. We must note that overall, the absolute values of ranks for the ADELI, STLBO, EBL SHADE, and TLBO algorithms differ only slightly, and the difference between the first and fourth ranks is often less than 0.5. The worst ranks are observed for PSO, NNA, CWOA, and WW.

It is known [89] that the Friedman, Friedman Aligned, and Quade tests are inadequate for establishing accurate comparisons between the considered algorithms. To compare a control method (one of 14 tested) with a set of other algorithms (the remaining 13), one can define a family of null hypotheses related to the control method. Applying a post-hoc procedure makes it possible to obtain a  $p$ -value that indicates

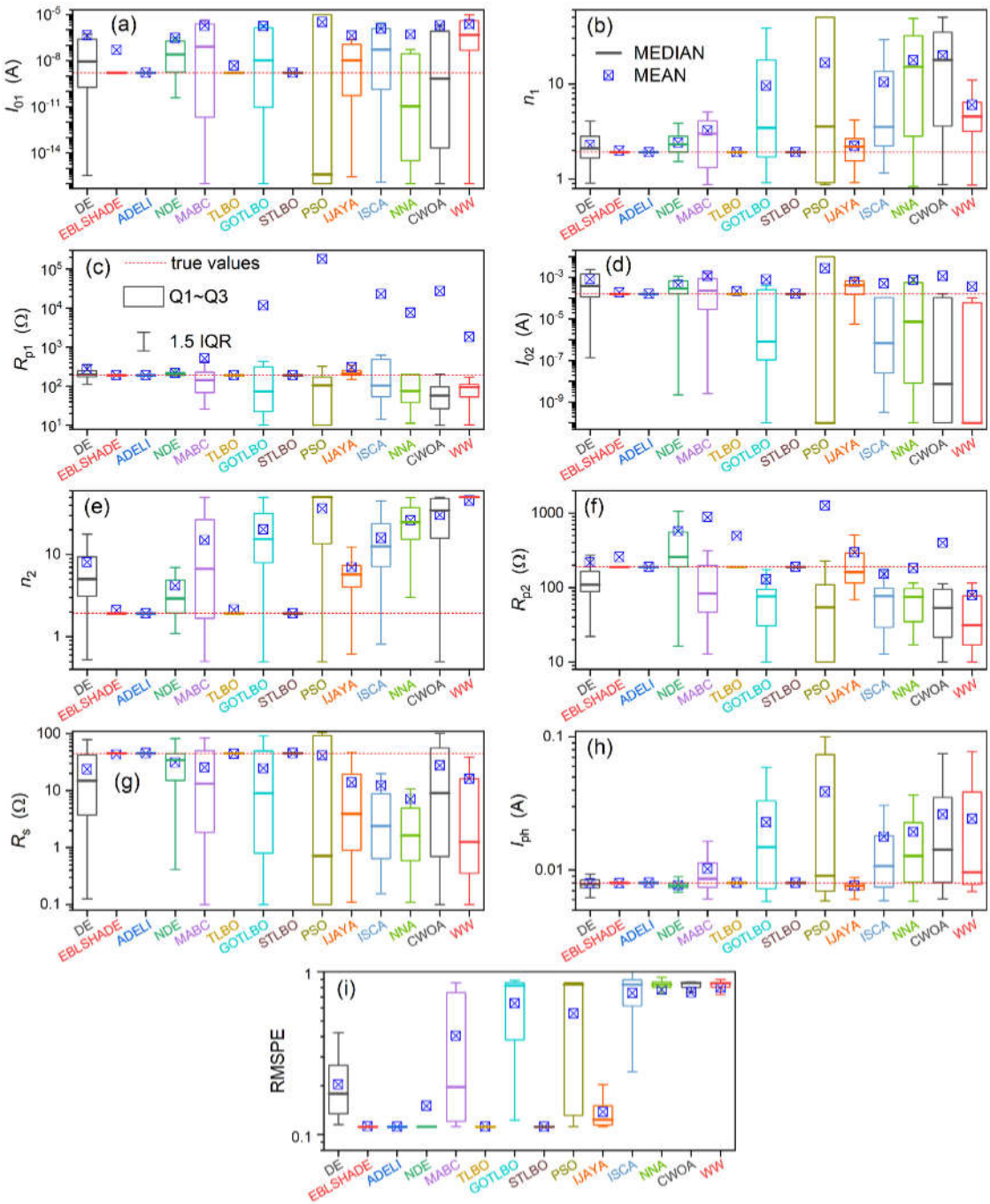


**Fig. 4.** Box-plots of  $I_{01}$  (a),  $n_1$  (b),  $R_{p1}$  (c),  $I_{02}$  (d),  $n_2$  (e),  $R_{p2}$  (f),  $R_s$  (g),  $I_{ph}$  (h), and RMSPE (i) estimation results by different optimization algorithms. The single-JV case. The squares represent the mean values, and the dashed lines correspond to the true parameter values.

the probability of obtaining the observed results if the corresponding hypothesis is true. We calculated  $p$ -values using four post-hoc procedures (Finner, Holm, Hochberg, and Holland) for all algorithms, tests, and tasks. The reader is referred to the supplementary material for all  $p$ -values (Tables S4–S143). In particular, a common feature of all comparisons is that the Finner post-hoc procedure demonstrates the most powerful behavior, yielding the lowest  $p$ -values.

In our study, we adopted a threshold value of  $p_{cr} = 0.1$  to establish a critical level for comparing the algorithms' effectiveness in both multiple  $1 \times N$  and  $N \times N$  comparisons. That is, it was defined that the likelihood of obtaining a result as extreme as the observed one if there is no difference between the two algorithms (null hypothesis), was less than 10%.

The statistical results of the comparison of algorithm effectiveness are available in the supplementary materials (figure S3). Among the compared algorithms, EBL SHADE, ADEL I, and STLBO consistently outperform the others in  $1 \times N$  multiple comparisons. On the other hand, algorithms such as PSO, ISCA, CWOA, and NNA consistently yield lower-quality results. The main changes observed in nonparametric statistical estimation of different parameters evaluation mainly concern algorithms with moderate effectiveness.

In all cases, the Quade test yields higher adjusted  $p$ -values. In particular, in the case of the complex parameter, the  $p$ -value for any comparison did not exceed the chosen threshold value  $p_{cr}$ .

The adjusted  $p$ -values obtained from the direct comparisons of EBL SHADE, ADEL I, and STLBO do not allow us to determine the best

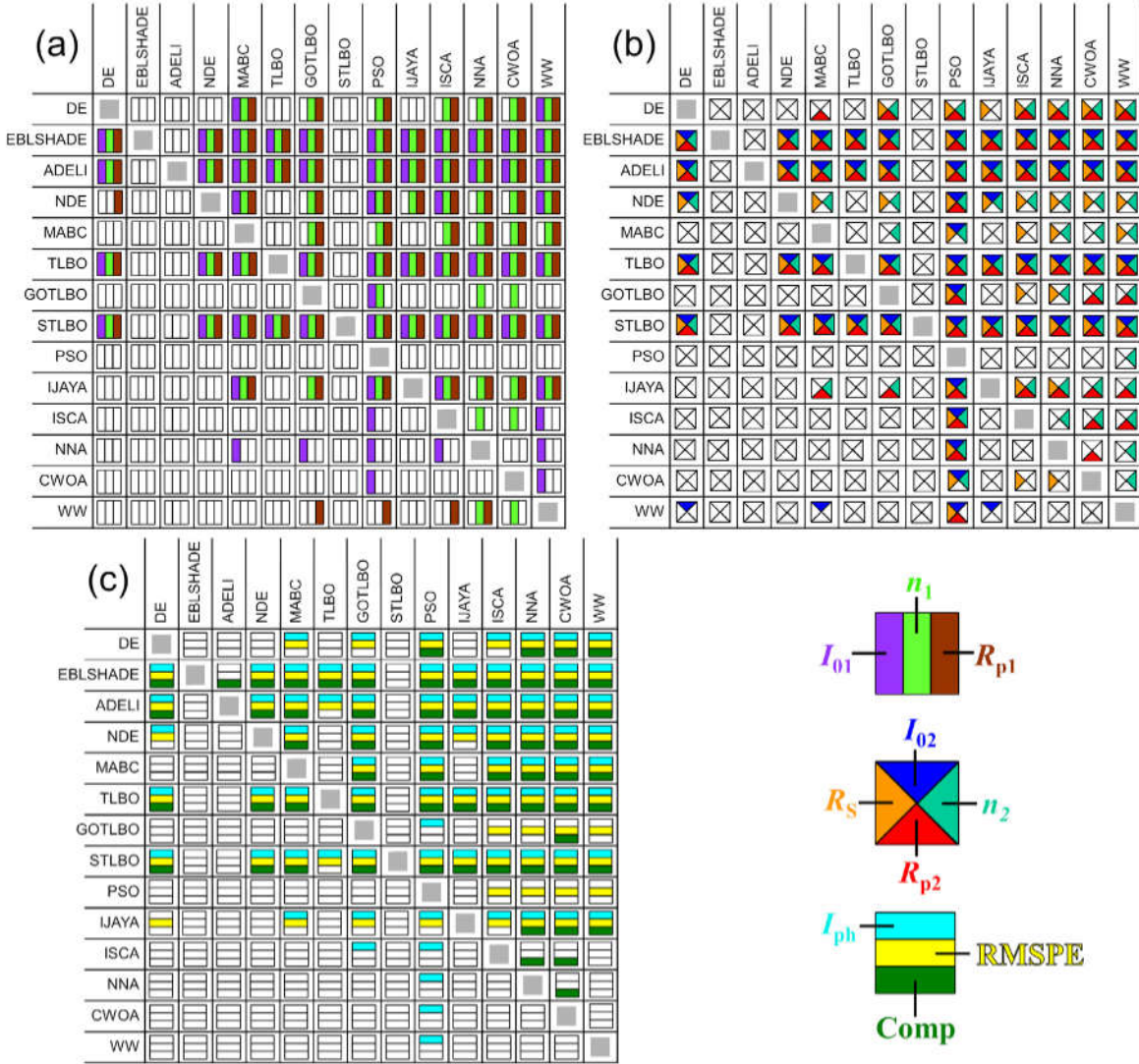


**Fig. 5.** The results of pairwise comparisons using the Wilcoxon signed-rank test for algorithms in the  $I_{01}$ ,  $n_1$ ,  $R_{p1}$  (a),  $I_{02}$ ,  $n_2$ ,  $R_s$  (b), and  $I_{ph}$  (c) extraction task, IV curve fitting (RMSPE value, c), the composite parameter Comp (c). A filled small rectangle (in panels a and b) or a triangle (in panel c) indicates that the algorithm listed in the row outperforms the algorithm listed in the column in one task. The correspondence between the position (color) of the rectangle (triangle) and the tested task is shown in a figure legend. A significance level of  $\alpha = 0.05$  was employed. The single-IV case. (For interpretation of the references to color in this figure legend, the reader is referred to the web version of this article.)

**Table 3**

The total count of wins and losses for each algorithm in  $1 \times N$  multiple comparisons using the Friedman, Friedman Aligned, and Quade tests, along with the Finner, Holm, Hochberg, and Holland post-hoc procedures in the single-IV case. The criterion for victory was an adjusted  $p$ -value of the null hypothesis less than 0.1. The best results in each task are bolded.

Algorithm	Wins/Loses										Total
	Task										
$I_{01}$	$n_1$	$R_{p1}$	$I_{02}$	$n_2$	$R_{p2}$	$R_s$	$I_{ph}$	RMSPE	Comp		
DE	24/43	56/34	48/35	4/73	48/43	49/34	49/40	45/35	49/48	16/27	388/412
EBL SHADE	<b>108/0</b>	<b>108/0</b>	<b>107/0</b>	<b>103/0</b>	<b>107/0</b>	<b>104/0</b>	<b>111/2</b>	<b>105/0</b>	<b>109/0</b>	<b>88/0</b>	1050/2
ADELI	<b>122/0</b>	<b>110/0</b>	<b>107/0</b>	<b>128/0</b>	<b>110/0</b>	<b>122/0</b>	<b>119/0</b>	<b>105/0</b>	<b>109/0</b>	<b>61/2</b>	<b>1093/2</b>
NDE	35/19	56/32	56/19	36/49	77/32	23/45	73/32	48/8	83/29	23/20	519/285
MABC	8/61	28/69	44/45	9/57	40/55	4/82	32/51	32/66	44/62	8/30	249/578
TLBO	80/3	102/0	101/0	84/13	99/0	87/18	93/10	<b>94/0</b>	<b>100/0</b>	65/2	905/46
GOTLBO	8/60	12/73	4/84	16/49	20/74	13/54	20/61	4/80	16/85	13/28	126/648
STLBO	<b>109/0</b>	<b>110/0</b>	<b>107/0</b>	<b>125/0</b>	<b>107/0</b>	<b>119/0</b>	<b>116/0</b>	<b>105/0</b>	<b>109/0</b>	<b>81/0</b>	1088/0
PSO	0/84	8/88	0/100	0/108	4/101	0/96	0/124	0/96	20/70	4/49	72/916
IJAYA	28/28	56/34	48/35	13/52	45/43	54/34	20/61	56/29	57/38	16/34	393/388
ISCA	8/56	12/76	4/84	12/45	28/65	16/51	8/61	17/68	0/92	16/32	121/630
NNA	33/29	0/92	4/84	12/49	12/84	12/57	8/77	12/80	0/92	0/52	93/696
CWOA	8/60	0/96	4/80	8/52	8/84	4/83	20/61	0/88	0/92	0/52	52/748
WW	0/96	12/76	16/76	36/43	0/108	10/60	12/77	12/66	0/92	0/52	98/844

**Table 4**  
Adjusted *p*-values for null hypotheses in  $I_{01}$  extraction task.  $N \times N$  multiple comparisons, single-*IV* case. Only *p*-values less than 1.0 are shown.

Comparison	Nemenyi procedure	Holm procedure	Shaffer's static procedure
ADELI versus WW	<1E-13	<1E-13	<1E-13
ADELI versus NDE	1.17195E-12	1.15907E-12	1.00453E-12
STLBO versus CWOA	1.17195E-12	1.15907E-12	1.00453E-12
TLBO versus PSO	1.21236E-12	1.17240E-12	1.03917E-12
STLBO versus GOTLBO	1.21236E-12	1.17240E-12	1.03917E-12
ADELI versus DE	1.73772E-12	1.64224E-12	1.48948E-12
STLBO versus DE	1.83875E-12	1.71752E-12	1.57607E-12
ADELI versus CWOA	3.83915E-12	3.50164E-12	3.29070E-12
EBLSHADE versus GOTLBO	4.20286E-12	3.78719E-12	3.60245E-12
STLBO versus NDE	5.01110E-12	4.46043E-12	4.29523E-12
ADELI versus GOTLBO	5.41522E-12	4.76064E-12	4.64162E-12
EBLSHADE versus CWOA	5.98099E-12	5.19229E-12	5.12657E-12
EBLSHADE versus ISCA	1.17195E-11	1.00453E-11	1.00453E-11
EBLSHADE versus DE	1.45282E-11	1.22931E-11	1.06966E-11
EBLSHADE versus NDE	4.17053E-11	3.43725E-11	3.07061E-11
STLBO versus ISCA	8.17133E-11	6.64482E-11	6.01625E-11
TLBO versus WW	8.82197E-11	7.07696E-11	6.49529E-11
TLBO versus MABC	1.07900E-10	8.53717E-11	7.94431E-11
EBLSHADE versus MABC	3.09961E-10	2.38431E-10	2.28213E-10
ADELI versus NNA	3.24570E-10	2.46102E-10	2.38969E-10
ADELI versus ISCA	3.83410E-10	2.86504E-10	2.82291E-10
STLBO versus MABC	1.58351E-09	1.16588E-09	1.16588E-09
STLBO versus NNA	1.83408E-09	1.33021E-09	1.33021E-09
TLBO versus ISCA	3.49326E-09	2.49519E-09	2.22648E-09
ADELI versus MABC	5.83612E-09	4.10452E-09	3.71972E-09
EBLSHADE versus NNA	1.23520E-08	8.55140E-09	7.87272E-09
EBLSHADE versus PSO	1.47150E-08	1.00256E-08	9.37877E-09
STLBO versus PSO	5.32586E-08	3.57008E-08	3.39450E-08
ADELI versus PSO	1.50038E-07	9.89261E-08	.56286E-08
TLBO versus GOTLBO	2.16253E-07	1.40208E-07	1.37831E-07
EBLSHADE versus WW	2.39169E-07	1.52438E-07	1.52438E-07
TLBO versus CWOA	2.89034E-07	1.81043E-07	1.77867E-07
TLBO versus DE	5.91345E-07	3.63905E-07	3.63905E-07
STLBO versus WW	6.86296E-07	4.14794E-07	4.14794E-07
TLBO versus NDE	1.37158E-06	8.13904E-07	7.68687E-07
TLBO versus NNA	1.17758E-04	6.72904E-05	6.59964E-05
NNA versus WW	2.21281E-02	1.24015E-02	1.24015E-02
IJAYA versus WW	2.36193E-01	1.29777E-01	1.24585E-01
NNA versus PSO	2.36193E-01	1.29777E-01	1.24585E-01
NDE versus WW	4.04596E-01	2.13413E-01	2.13413E-01
DE versus WW	6.28685E-01	3.24706E-01	3.24706E-01
CWOA versus WW	8.94683E-01	4.52257E-01	4.52257E-01
GOTLBO versus WW	1.0	5.07626E-01	5.07626E-01
IJAYA versus PSO	1.0	8.15876E-01	7.97333E-01
NNA versus MABC	1.0	9.64793E-01	9.64793E-01

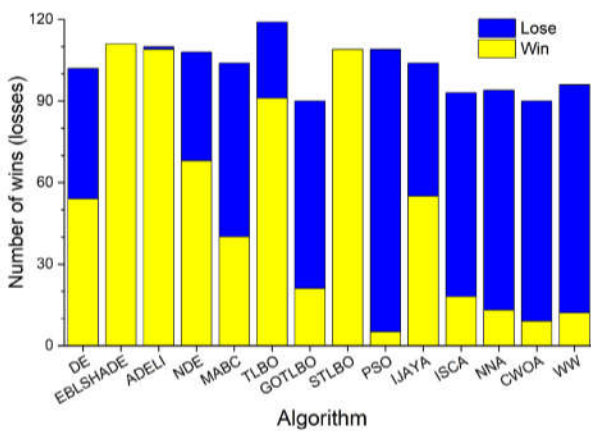


**Fig. 6.** The total count of wins (height of the bottom of the bars) and losses (height of the top of the bars) for each algorithm in pairwise comparisons conducted using the Wilcoxon signed-rank test at a significance level of  $\alpha = 0.05$  in the single-*IV* case.

algorithm among them. However, we can use the results of these top three algorithms, obtained from their comparisons with less efficient optimization methods, for this purpose.

**Table 3** summarizes the counts of wins and losses for each algorithm in  $1 \times N$  multiple comparisons. The maximum possible number of wins achieved in every 10 tasks is 156, obtained from comparisons with 13 algorithms across 3 tests using 4 procedures. Among the compared algorithms, ADELI showed the highest number of statistically significant improvements (1093) over others, indicating its superior performance. Conversely, STLBO demonstrated the lowest number of defeats (0) in similar comparisons, suggesting its consistently strong performance.

The results above show the outcomes of the procedures used to control the Family-Wise Error Rate (FWER) for comparisons with a control algorithm. We individually tested each of the 14 algorithms to determine if any of them were superior to the others. The results below display the multiple comparisons carried out, involving the computation of all possible pairwise comparisons ( $N \times N$  comparison). Three procedures (Shaffer's static, Nemenyi, and Holm) were employed to control FWER. These methods consider that the hypotheses being tested belong to a family of all pairwise comparisons and are logically interrelated; thus, not all combinations of true and false hypotheses are possible.

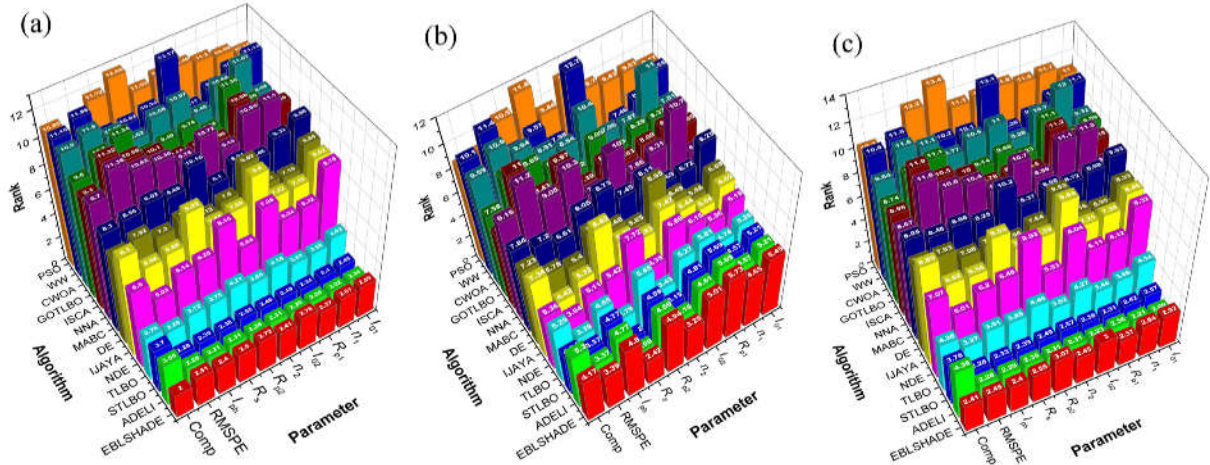


**Fig. 7.** The ranking of algorithms in various tasks based on the Friedman (a), Friedman Aligned (b), and Quade (c) tests in the single-JV case.

Starting from the analysis performed by the Friedman test on our results, we can raise the 91 null hypotheses of equality among the 14 algorithms in our study for each task and apply the previously mentioned procedures to contrast them.

**Table 4** lists a portion of the hypotheses and the adjusted *p*-values achieved for the task of  $I_{01}$  estimation. For the remaining 46 hypotheses not indicated in the table, a *p*-value of 1 was obtained after applying each of the procedures. The full version of the table, as well as the data obtained for other tasks, are given in the supplementary material (tables S144–S153).

It can be seen that at a significance level of 0.1, only 37 hypotheses of equality are rejected by the Nemenyi, Holm, and Shaffer methods. These hypotheses show the improvement of EBL SHADE, ADELI, TLBO, and STLBO over DE, NDE, MABC, GOTLBO, PSO, ISCA, NNA, CWOA, and WW, as well as NNA over WW. None of the remaining 54 hypotheses can be rejected using these procedures.

It should be noted that when testing complementary hypotheses (“algorithm A vs algorithm B” and “algorithm B vs algorithm A”), a *p*-value less than 1 can be obtained in only one of the two cases. For instance, when using the Nemenyi procedure to  $I_{01}$  evaluating by comparing “ADELI vs MABC”, a *p*-value of  $5.84 \cdot 10^{-9}$  was obtained. Conversely, when comparing “MABC vs ADELI”, the *p*-value was 1. The *p*-values were computed for all possible hypotheses in the study to identify algorithms whose results statistically deviate from those of other algorithms. In this case, a critical value of  $p_{cr} = 0.1$  was used, similar to the  $1 \times N$  multiple comparisons. Typical examples of the obtained results for specific parameter cases are presented in **Fig. 8**. Please refer to figure S4 in the supplementary materials for more detailed and comprehensive data. Generalized results regarding the total count of victories and defeats in the  $N \times N$  comparisons are listed in **Table 5**. In the case of  $N \times N$  comparisons, the maximum possible number of wins achieved in every 10 tasks is 39, obtained from comparing 13 algorithms in 3 post-hoc procedures.

In most instances, all post-hoc procedures considered lead to similar conclusions regarding the outperformance of one algorithm over another. For example, in the case of the  $R_{p1}$  estimation task, the Nemenyi procedure disagrees with the Holm and Shaffer methods in only 4 out of 57 cases. Particularly, this happens for the comparisons “DE vs WW”, “MABC vs ISCA”, “MABC vs NNA”, and “TLBO vs NDE” — see **Fig. 8(a)**. On the other hand, as evident from **Fig. 8(b)**, such situations are not observed at all for the  $I_{02}$  evaluation task. In general, the results of the Holm procedure differ from those of the Shaffer procedure in only two comparisons: the improvement of IJAYA over GOTLBO in the  $n_1$  estimation and the outperformance of TLBO over NNA for the composite parameter.

Totally  $1 \times N$  multiple comparisons exhibit more powerful behavior than  $N \times N$  ones, resulting in lower *p*-values. As a result, IJAYA did not lose in any of the  $N \times N$  comparisons — see **Table 5**. Another striking example can be observed when considering the case of the composite parameter. Based on the  $1 \times N$  comparisons, conclusions were drawn about the outperformance of one algorithm over another in 67 cases, whereas for the  $N \times N$  comparisons, such situations were identified in only 20 cases: the improvement of EBL SHADE over MABC, GOTLBO, PSO, ISCA, NNA, CWOA, and WW, the statistically significant difference ADELI and GOTLBO, PSO, NNA, CWOA, and WW, and outperformance of both TLBO and STLBO over PSO, NNA, CWOA, and WW. As a result,  $N \times N$  comparisons yield a less precise ranking of all algorithms. Nonetheless, it remains feasible to discern the best and worst-performing algorithms. The data obtained reveal that EBL SHADE, ADELI, and STLBO consistently emerge as the top-performing algorithms across all tasks, while PSO, ISCA, NNA, CWOA, and WW consistently rank among the worst performers.

Thus, the results presented in this subsection demonstrate that no examined algorithm can be defined as one that allows for precisely estimating only one (e.g., only  $R_{p2}$  or only  $I_{02}$ ) parameter in the opposed two-diode model. The algorithms that exhibit high efficiency (EBL SHADE, ADELI, and STLBO) allow for the most precise estimation of all parameters. However, certain algorithms indeed display higher accuracy in determining specific parameters. Indeed, DE and IJAYA are the most effective in estimating  $R_{p2}$  and  $I_{ph}$  as shown in **see table S1**. Nevertheless, this highest level of accuracy appears not worth significant attention when compared to other optimization methods. As a result, the performance metrics of algorithms for individual parameter evaluation will not be analyzed in the following subsection, which is dedicated to the analysis of JV curves with different parameter ratios.

### 3.3.2. Parameter extraction in JV-set case

**Fig. 3** shows several typical fitting results of a set of synthetic JV curves simulated according to the opposed two-diode model using the parameter values described in Section 2.2.2. A more comprehensive and enhanced version, including the fitting results obtained using each algorithm, is provided in the supplementary materials (figure S5). Similar to the single-JV case, the algorithms EBL SHADE, ADELI, NDE, IJAYA, TLBO, and STLBO demonstrate the highest agreement between the fitting curves and the points of simulated current–voltage curves. **Fig. 9** represents a portion of the results obtained from evaluating solar cell parameters using various algorithms, as well as the corresponding RMSPE data. The supplementary material contains the temperature dependencies of all parameters determined by all algorithms applied (figures S6–S14) and scatter plots, which depict the relationship between all model parameters’ true and evaluated values

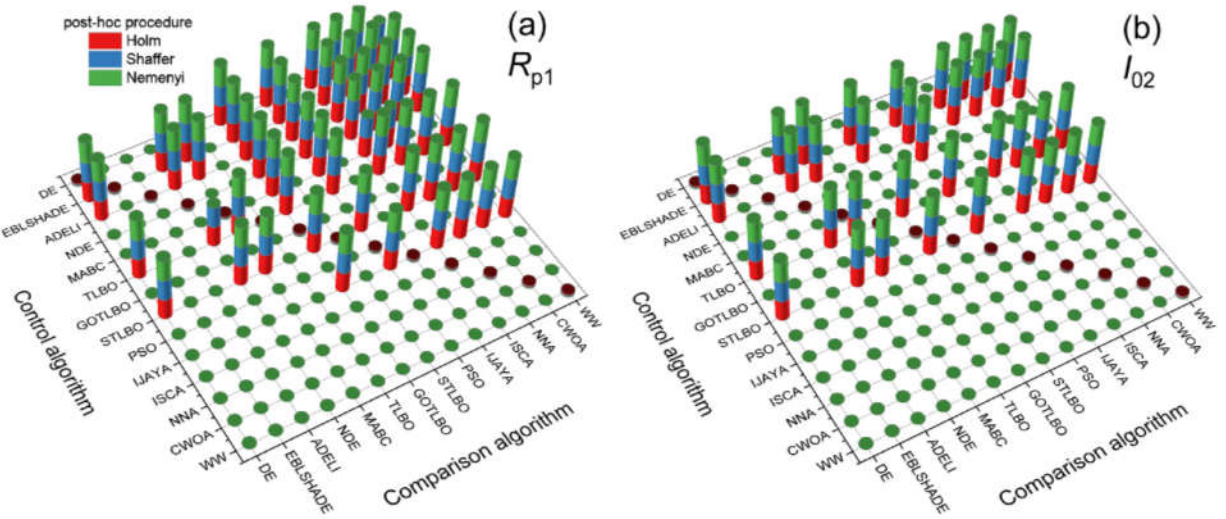


**Fig. 8.** The results of  $N \times N$  multiple comparisons using Friedman test with Shaffer's static, Nemenyi, and Holm procedures for algorithms in the  $R_{p1}$  (a) and  $I_{02}$  (b) extraction task. The presence of colored cylinder indicates that the adjusted  $p$ -value of the null hypothesis for comparison “control algorithm vs comparison algorithm” less than  $p_{cr} = 0.1$ . The correspondence between the color of the cylinder and the post-hoc procedure is shown in a figure legend. The single- $JV$  case. (For interpretation of the references to color in this figure legend, the reader is referred to the web version of this article.)

**Table 5**

The total count of wins and losses for each algorithm in  $N \times N$  multiple comparisons using the Friedman test with Shaffer's static, Nemenyi, and Holm procedures in single- $JV$  case. The criterion for victory was an adjusted  $p$ -value of the null hypothesis less than 0.1. The best results are bolded.

Algorithm	Wins/Loses										Total	
	Task											
	$I_{01}$	$n_1$	$R_{p1}$	$I_{02}$	$n_2$	$R_{p2}$	$R_s$	$I_{ph}$	RMSPE	Comp		
DE	0/12	17/12	17/12	0/12	12/12	14/12	5/12	17/12	15/15	0/0	97/111	
EBLSHADE	27/0	27/0	27/0	27/0	27/0	27/0	27/0	27/0	26/0	21/0	<b>263/0</b>	
ADELI	27/0	27/0	27/0	27/0	27/0	27/0	27/0	27/0	27/0	14/0	<b>257/0</b>	
NDE	0/12	21/12	18/11	3/12	18/9	3/12	18/11	21/9	24/8	0/0	126/96	
MABC	0/12	0/15	10/12	0/12	11/12	0/17	3/12	2/15	12/15	0/3	38/125	
TLBO	27/0	27/0	26/0	27/0	24/0	27/0	26/0	24/0	24/0	10/0	242/0	
GOTLBO	0/12	0/18	0/24	0/12	3/15	0/12	3/15	0/21	0/21	0/5	6/155	
STLBO	27/0	27/0	27/0	27/0	27/0	27/0	27/0	27/0	27/0	11/0	<b>254/0</b>	
PSO	0/12	0/21	0/24	0/15	0/24	0/21	0/34	0/23	0/18	0/12	0/204	
IJAYA	0/0	16/0	18/0	0/0	12/0	11/0	3/0	18/0	18/0	0/0	96/0	
ISCA	0/12	0/21	0/23	0/12	3/15	0/12	2/15	0/21	0/24	0/3	5/158	
NNA	3/12	0/21	0/23	0/12	0/23	0/14	0/17	0/21	0/24	0/9	3/176	
CWOA	0/12	0/21	0/21	0/12	0/24	0/18	3/15	0/21	0/24	0/12	3/180	
WW	0/15	0/21	0/20	0/12	0/30	0/18	2/15	0/20	0/24	0/12	2/187	

(figures S15–S22). The results, including MEAN, MEDIAN, STD, and IQR, are also tabulated (table S154 in the supplementary material).

It should be noted that in several cases, the accuracy of parameter estimation depends on temperature, even for constant parameters. For instance, as the temperature increases, the errors in determining  $R_{p1}$  decrease for NDE, MABC, GOTLBO, IJAYA, ISCA, and WW. However, under the same conditions, the estimation quality of  $I_{01}$  worsens using DE, ISCA, and WW. These results indicate that some parameter determination accuracy depends on the value of this parameter and other parameter values. However, the specific dependencies of parameter estimation accuracy for each algorithm were beyond the scope of the study. We aimed to determine the best algorithms only.

The presented data display several features similarly found in the single- $JV$  case. For instance, the error in parameter estimation by mean values is higher than median value errors in most instances. Exceptions arise at some temperatures, particularly when evaluating  $I_{01}$  using IJAYA,  $n_1$  using IJAYA and DE,  $R_{p1}$  using DE and MABC, and  $R_s$  using DE and WW. However, with high-precision algorithms, the deviation of MEDIAN from the true value does not exceed that of MEAN. Additionally, these algorithms exhibit small IQR values that do not exceed STD. Similar to the previous case, small RMSPE values do

not always indicate high accuracy in determining the parameters of a solar cell.

At the same time, the number of algorithms exhibiting minimal errors has decreased. Significant deviations from true values are observed for median values of  $I_{01}$ ,  $n_1$ ,  $R_{p1}$ ,  $n_2$ ,  $R_s$ , and  $I_{ph}$  evaluated by EBL SHADE at various temperatures, as well as for median values of diode D1 characteristics and series resistor determined using TLBO at 260 K. Thus, only ADELI and STLBO remain as algorithms without visible errors. Although this claim of infallibility applies only to median values, substantial errors are observed for mean values in several cases. Simultaneously, EBL SHADE, TLBO, IJAYA, and NDE constitute a group of algorithms with low RMSPE values but imperfect model parameter estimation.

In the  $JV$ -set case, to assess the statistical performance of compared algorithms, the run time and all  $\text{APE}_{\text{MEDIAN}}$  and  $\text{RMSPE}_{\text{MEDIAN}}$  values for each  $JV$  curve were taken into account. This approach mirrors the use of the Comp parameter in the previous subsection; however, in this scenario,  $N_{pr} = 81$  is employed:

$$N_{pr} = 10 T_{\text{values}} \times (8 \text{APE}_{\text{MEDIAN}} + 1 \text{RMSPE}_{\text{MEDIAN}}) + 1 t_{\text{run}}.$$

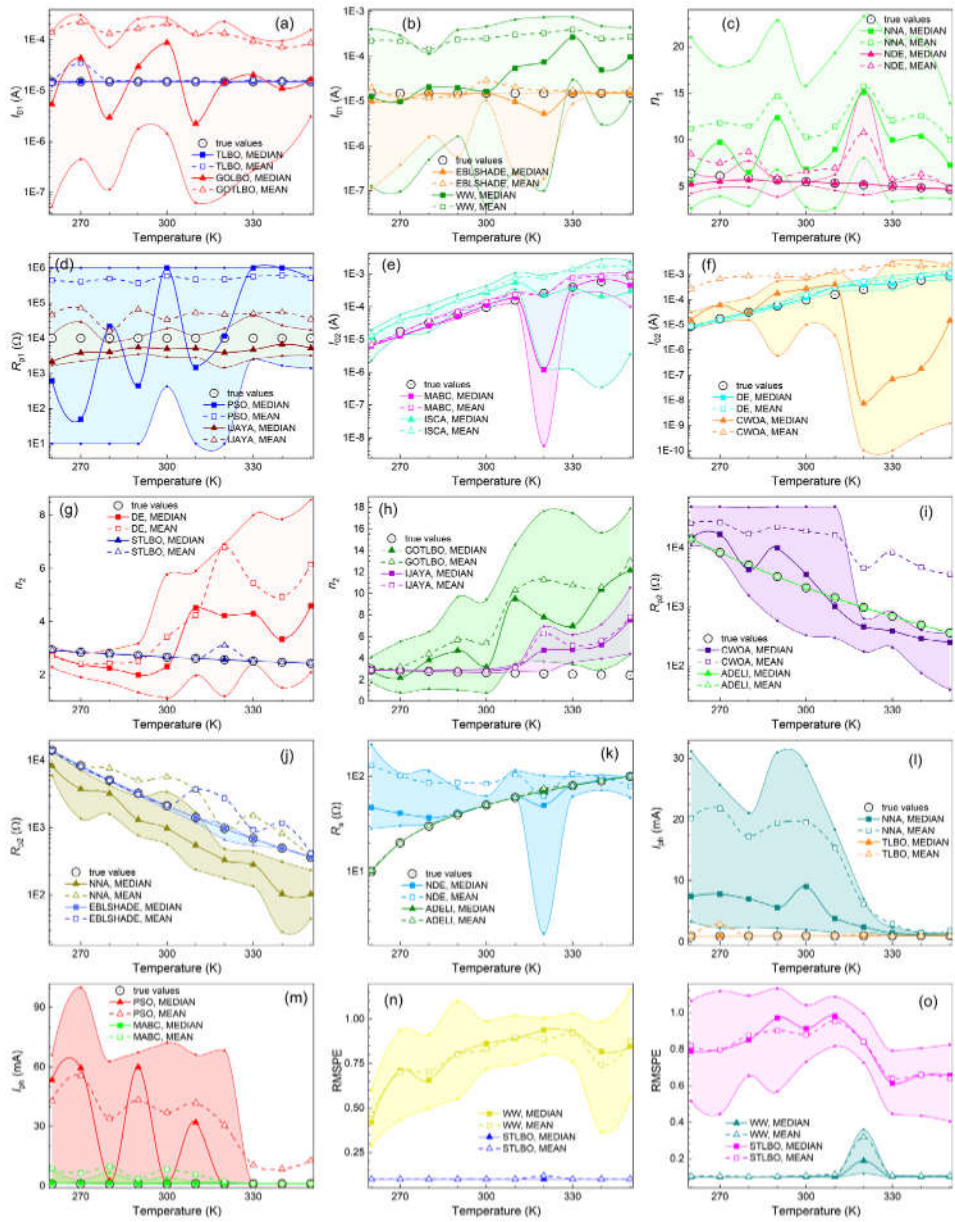


**Fig. 9.** The dependencies of the  $I_{01}$  (a, b),  $n_1$  (c),  $R_{p1}$  (d),  $I_{02}$  (e, f),  $n_2$  (g, h),  $R_{p2}$  (i, j),  $R_s$  (k),  $I_{ph}$  (l, m), and RMSPE (n, o) values on the temperature of IV simulation in the IV-set case are obtained using TLBO (a, l), GOTLBO (a, h), EBLSHADE (b, j), WW (b, n, o), NNA (c, j, l), NDE (c, k), PSO (d, m), IJAVA (d, h), MABC (e, m), ISCA (e), DE (f, g), CWOA (f, i), STLBO (g, n, o), and ADELI (i, k) algorithms. Circles represent the values used in IV curve simulations. Filled marks indicate the median values, while empty marks indicate the mean values. The colored regions correspond to the IQR. The lines serve only as a guide to the eye. (For interpretation of the references to color in this figure legend, the reader is referred to the web version of this article.)

Therefore, this approach is well-suited for nonparametric statistical analysis of  $k = 14$  meta-heuristic algorithms. Certainly, at first glance, it would be interesting to consider incorporating an additional 80 values of the interquartile range into the dataset. This strategy could offer insight into the stability of algorithm performance as well. However, it is known [89] that for multiple comparisons, a value of  $N_{pr} \geq 8 \cdot k = 112$  could be too high, resulting in no significant comparisons.

Table 6 presents the statistical results generated by the Wilcoxon test. According to the table, ADELI outperforms all other algorithms with a significance level of  $\alpha = 0.05$ . STLBO and TLBO demonstrate improvements over DE, EBLSHADE, NDE, MABC, GOTLBO, PSO, IJAVA, CWOA, NNA, and WW.

The counts of statistically significant cases (+/- = /-) are presented in the last row of Table 6. It can be seen that PSO, ISCA, NNA, and CWOA did not outperform any of the algorithms, whereas WW statistically significantly improved over NNA only. Therefore, although

these algorithms boast promising run times, they are not recommended for SC parameter estimation based on the opposed two-diode model.

The  $p$ -values required to test the null hypothesis, computed using the Friedman, Friedman Aligned, Quade tests, and the Iman–Davenport extension, can be found in table S2 of the supplementary materials. None of these values exceeds  $2.3 \cdot 10^{-6}$ , thus rejecting the hypothesis of equivalent medians in all tests.

Ranks achieved by the Friedman, Friedman Aligned, and Quade tests are shown in Fig. 10 and table S3 (supplementary material). According to the given results, ADELI has been placed first by the Friedman and Quade tests, while STLBO has ranked first by the Friedman Aligned test.

Ranks achieved by the Friedman, Friedman Aligned, and Quade tests are shown in Fig. 10 and table S3 in the supplementary material. As per the given results, ADELI has been placed at first rank by Friedman and Quade tests, and STLBO has ranked first by the Friedman

**Table 6**

Pairwise comparison results of algorithms using the Wilcoxon signed-rank test with a level of significance  $\alpha = 0.05$  in the IV-set case. A “+” indicates that the null hypothesis was rejected, and the control algorithm (listed in the row) outperformed the comparison algorithm (listed in the column). The “0” indicates the rejection of the hypothesis about better performing the control algorithm. The last column contains the total number of wins (when the algorithm listed in the row was the control, indicated by “+”), the total number of losses (when the algorithm was the comparison, indicated by “-”), and the number of comparisons where the hypothesis of equal algorithm effectiveness was not rejected (indicated by “=”).

Control	Comparison algorithm												(+/ = /-)		
	DE	EBL SHADE	ADELI	NDE	MABC	TLBO	GOTLBO	STLBO	PSO	IJAYA	ISCA	NNA	CWOA		
DE	■ 0	0	0	0	+	0	+	0	+	0	+	+	+	+	7/0/6
EBL SHADE	+	■	0	+	+	0	+	0	+	+	+	+	+	+	10/0/3
ADELI	+	+	■	+	+	+	+	+	+	+	+	+	+	+	13/0/0
NDE	+	0	0	■	+	0	+	0	+	+	+	+	+	+	9/0/4
MABC	0	0	0	0	■	0	+	0	+	0	+	+	+	+	6/0/7
TLBO	+	+	0	+	+	■	+	0	+	+	+	+	+	+	11/1/1
GOTLBO	0	0	0	0	0	0	■	0	+	0	+	+	+	+	5/0/8
STLBO	+	+	0	+	+	0	+	■	+	+	+	+	+	+	11/1/1
PSO	0	0	0	0	0	0	0	0	■	0	0	0	0	0	0/4/9
IJAYA	+	0	0	0	+	0	+	0	+	■	+	+	+	+	8/0/5
ISCA	0	0	0	0	0	0	0	0	0	0	■	0	0	0	0/3/10
NNA	0	0	0	0	0	0	0	0	0	0	0	■	0	0	0/3/10
CWOA	0	0	0	0	0	0	0	0	0	0	0	0	■	0	0/4/9
WW	0	0	0	0	0	0	0	0	0	0	0	+	0	■	1/3/9

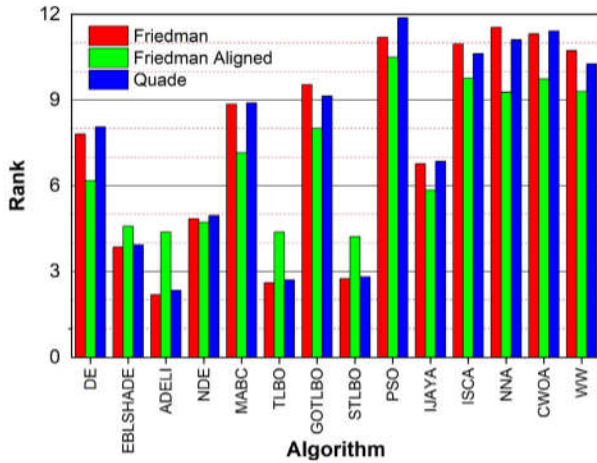


**Fig. 10.** Algorithms' ranks according to the Friedman, Friedman Aligned, and Quade tests in the IV-set case.

**Table 7**

The total count of wins and losses for each algorithm in  $1 \times N$  and  $N \times N$  multiple comparisons using all tests with all post-hoc procedures in the IV-set case. The criterion for victory was an adjusted  $p$ -value of the null hypothesis less than 0.1. The best results are bolded.

Algorithm	Wins/Loses	
	$1 \times N$ comparisons	$N \times N$ comparisons
DE	44/53	15/15
EBL SHADE	100/6	24/0
ADELI	117/0	<b>27/0</b>
NDE	97/18	24/9
MABC	44/69	14/18
TLBO	111/0	<b>27/0</b>
GOTLBO	25/80	2/18
STLBO	<b>118/0</b>	<b>27/0</b>
PSO	0/112	0/24
IJAYA	63/46	21/0
ISCA	4/97	0/24
NNA	12/93	0/26
CWOA	4/101	0/24
WW	12/80	0/23

Aligned test. TLBO has been recorded as the second-best algorithm by all three tests. Furthermore, PSO was identified as the worst-performing algorithm by the tests' unanimous decision.

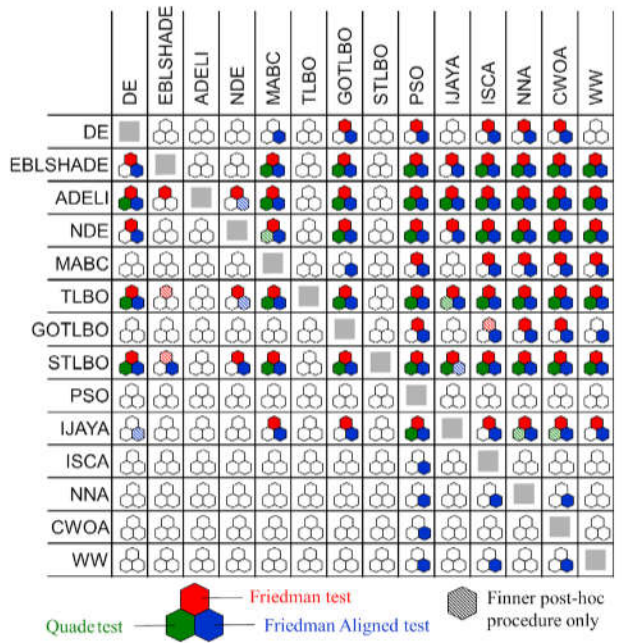


**Fig. 11.** The results of algorithms in  $1 \times n$  multiple comparisons using the Friedman, Friedman Aligned, and Quade tests in the IV-set case. A solid filled hexagon indicates that the  $p$ -value of the null hypothesis for the comparison “algorithm in a row versus algorithm in a column”, obtained using one of the tests and all post-hoc procedures, are less than  $p_{cr} = 0.1$ . The shaded hexagon indicates that  $p < p_{cr}$  in the case of the Finner post-hoc procedure only. The correspondence between the position (color) of the hexagon and the test is shown in a figure legend. (For interpretation of the references to color in this figure legend, the reader is referred to the web version of this article.)

The  $p$ -values obtained for  $1 \times N$  multiple comparisons are shown in tables S155–168 (supplementary material). These are the results of applying the Finner, Holm, Hochberg, and Holland procedures, as a post-hoc method after the Friedman, Friedman Aligned, and Quade tests. Additionally, Shaffer, Nemenyi, and Holm post-hoc procedures were applied after the Friedman test for  $N \times N$  multiple comparisons, and the corresponding  $p$ -values can be found in table S169 (supplementary material). The results of determining whether one algorithm yielded a statistically better estimation of parameters than another (with  $ap$ -value  $\leq p_{cr} = 0.1$ ) are summarized in Figs. 11 and 12 for  $1 \times N$  and  $N \times N$  comparisons, respectively. The counts of statistically significant cases are listed in Table 7.

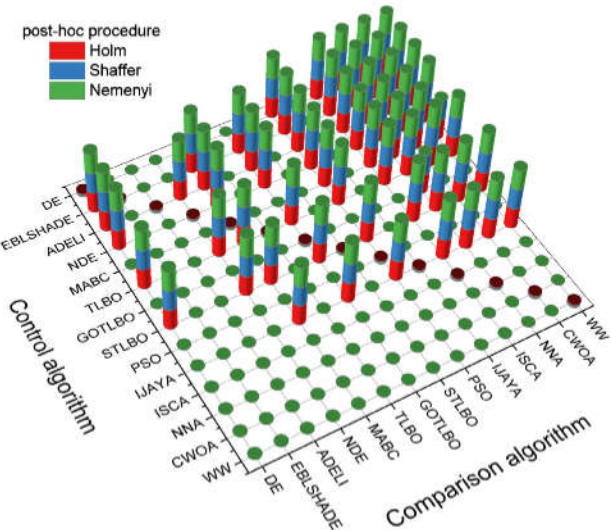


**Fig. 12.** The results of  $N \times N$  multiple comparisons using Friedman test with Shaffer's static, Nemenyi, and Holm post-hoc procedures for algorithms in the IV-set case. The presence of colored cylinder indicates that the adjusted  $p$ -value of the null hypothesis for comparison "control algorithm vs comparison algorithm" less than  $p_{cr} = 0.1$ . The correspondence between the color of the cylinder and the post-hoc procedure is shown in a figure legend. (For interpretation of the references to color in this figure legend, the reader is referred to the web version of this article.)

As can be seen, ADELI, TLBO, and STLBO were never outperformed by any other algorithms in both  $1 \times N$  and  $N \times N$  multiple comparison cases. Additionally, the same property (unbeaten) is observed with EBL SHADE and IJAYA for  $N \times N$  comparisons as well. Overall, the parameter estimation results obtained from the set of IV curves in the opposed two-diode model using ADELI, TLBO, and STLBO algorithms are practically indistinguishable in  $N \times N$  comparisons (differences in  $p$ -values are very small). In  $1 \times N$  comparisons, TLBO shows lower performance than ADELI and STLBO. The improvement of TLBO over EBL SHADE is proved only by the Finner procedure applied in the Friedman test. Based on  $1 \times N$  comparisons, slight differences between ADELI and STLBO are observed, especially for comparisons versus the non-worst algorithms. For example, the Quade test confirms ADELI's improvement over EBL SHADE across all post-hoc procedures. However, neither the Friedman test nor the Friedman Aligned test showed statistically significant differences between these algorithms. Meanwhile, the Quade and Friedman Aligned tests reveal differences between STLBO and EBL SHADE for only the Finner procedure and every post-hoc procedure, respectively. Regarding comparison with NDE, the Friedman Aligned test demonstrated that STLBO is better than NDE according to all post-hoc procedures. In contrast, the ADELI outperformance over NDE was only observed using the Finner method. In the case of comparisons versus IJAYA, the results of the Friedman Aligned test show a reversal: only the Finner procedure indicates an STLBO advantage, whereas ADELI outperforms IJAYA according to all utilized post-hoc methods.

When deciding on the optimal algorithm for SC parameter extraction from the IV curve using the opposed two-diode model, one must choose between EBL SHADE, ADELI, TLBO, and STLBO in fact. However, TLBO exhibited lower performance when applied to the single-IV case. The parameter evaluation error when using EBL SHADE was not always minimal in the IV-set case. Despite the minimal advantage in terms of win counts in  $1 \times N$  comparisons (see Table 7), we hesitate to declare STLBO as the best. We believe STLBO and ADELI jointly hold the top position in this study's competition.

Over the last few decades, researchers have strived to enhance the performance of metaheuristic algorithms using various concepts,

including [17]: hybridization between two or more metaheuristics, quantum computing concept, opposition-based theory, chaotic maps, Lévy-Flight strategy. Our research has revealed that the most promising approaches to solving the parameter estimation problem for S-shaped IV curves involve the use of enhanced mutation strategies. Specifically, this entails employing chaotic maps to tune mutation coefficients and utilizing the elite strategy (STLBO). Furthermore, highly productive results were achieved through the application of nonlinear (polynomial) approximation of potential solutions (ADELI).

When analyzing the significance of the results, it is essential to consider the following points. The IV characteristics are one of the key measurements in the analysis of solar cells in both research and industrial mass production. Typically, IV curves are analyzed using a specific model, and the model parameters are closely related to the internal physical mechanisms acting within the solar cell. Therefore, their efficient and sufficiently accurate extraction is important as an analysis tool for understanding the processes involved. Thus, the algorithms selected in our study can significantly aid in modeling NG-SCs, aiming to enhance the understanding of their internal processes. Specifically, this includes the underlying causes of the S-shaped kink and the peculiarities of PV conversion in advanced solar cells, such as those employing phase-change materials [91,92].

Precise knowledge of the model parameter values is crucial for many practical applications. For example, they are used in the simulation and emulation of PV systems, for quality control of PV cells during manufacturing, and in the study of SC degradation [93]. So, for a successful implementation of a PV system, the availability of an accurate, fast, and reliable computer simulation tool is indispensable. The algorithm for model parameter extraction can be a valuable tool for developing a reliable computational engine for a PV simulator [94]. Diagnosing PV degradation can be achieved by monitoring and comparing the SC parameters with those in their initial states. In this case, it is impossible to overstate the importance of the ability to parameter extraction with high precision. Finally, optimization efforts and quantitative studies to assess the capabilities of a particular technology greatly benefit from the correct extraction of the model parameters under various test conditions [95]. Implementing selected algorithms in real-world solar cell testing and production environments allows for enhanced characterization precision (due to precise determination of model parameters), production process optimization (more accurate SC characterization leads to minimizing defects and increasing efficiency), quality improvement (the algorithm helps identify shortcomings at early production stages, thereby enhancing overall product quality), testing acceleration (the automated model parameter determination can shorten the time required for testing each element, enabling increased production volumes), and cost reduction (optimizing the testing process and reducing the number of defective elements decreases production costs). Moreover, potential challenges in deployment are minimal, given the algorithms' low resource requirements and compatibility with modern computers. There is no need for personnel training, as understanding the intricacies of the algorithms is unnecessary for their use. Additionally, constant maintenance, updates, and bug fixes are not required. The only requirements for implementation involve developing software interfaces to integrate the new algorithms with existing control and monitoring systems and ensuring the market's readiness to adapt established processes to these changes.

#### 4. Conclusion

This paper explores the feasibility of employing meta-heuristic algorithms to address parameter extraction challenges of photovoltaic cells exhibiting S-shaped current-voltage characteristics. The parameter evaluation is carried out within the framework of the opposed two-diode model. A total of 14 meta-heuristic algorithms from diverse classes are implemented to extract solar cell parameters from synthetic IV curves, which have been initially generated by using a wide range

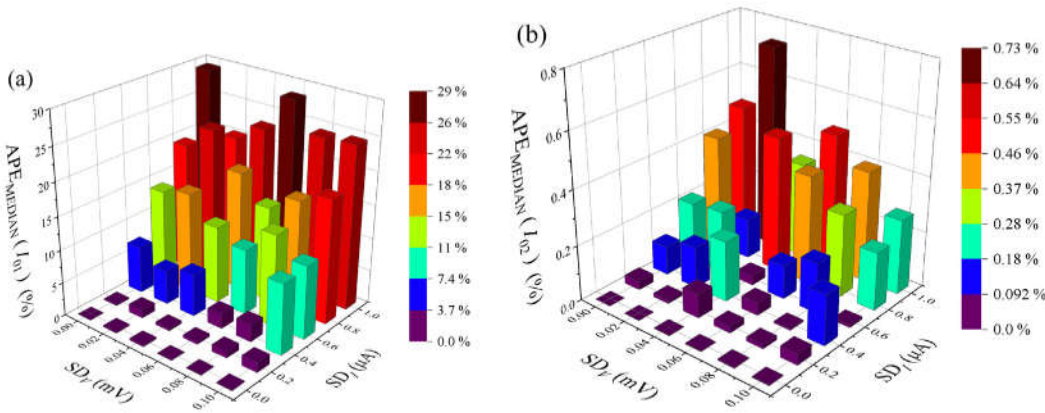


**Fig. 13.** The accuracy of the  $I_{01}$  (a) and  $I_{02}$  (b) evaluations from noisy IV curves versus voltage and current standard deviations. The APE<sub>MEDIAN</sub> values were averaged over 100 IV curves, all simulated with equal values of  $SD_V$  and  $SD_I$ . (For interpretation of the references to color in this figure legend, the reader is referred to the web version of this article.)

of parameter values. The results are compared using nonparametric statistical procedures, including pairwise comparisons,  $1 \times N$  multiple comparisons, and  $N \times N$  multiple comparisons.

Research has shown that employing a square error-based fitness function provides clear advantages in addressing the given problem compared to an absolute error-based fitness function. The overall results of various algorithms' performance align with the No Free Lunch theorem. GOTLBO, PSO, ISCA, NNA, CWOA, and WW are entirely unsuitable for parameter evaluation using the opposed two-diode model. The results of DE, NDE, MABC, and IJAYA are not as subpar as those in the previous group; however, overall, it is not advisable to utilize these algorithms for parameter extraction. In general, EBL SHADE and TLBO prove effective in accurately determining parameter values in most instances. However, investigation has revealed that these algorithms may falter under certain conditions. Thus, caution is warranted when applying EBL SHADE and TLBO to solar cells with S-shaped IV curves. In conclusion, STLBO and ADELI exhibit superior performance in accuracy and reliability compared to other algorithms. In particular, these two algorithms successfully determine parameters from similar IV curves corresponding to photovoltaic cells with distinct characteristics.

It is worth noting that in this study, the parameters were obtained from idealized IV curves, where the voltage–current relationships have been precisely defined by Eq. (1). In an actual experiment, there is potential for errors in both current and voltage measurements. Therefore, it would be valuable to investigate the effectiveness of various meta-heuristic algorithms in determining parameters from IV data corrupted by noise in future research (the results of some preliminary simulations are presented in Appendix A).

This work involving testing and comparative analysis of various meta-heuristic algorithms for estimating solar cell parameters should significantly contribute to further research and development in photovoltaic systems.

#### CRediT authorship contribution statement

**Oleg Olikh:** Writing – review & editing, Writing – original draft, Visualization, Validation, Software, Resources, Investigation, Formal analysis, Data curation, Conceptualization.

#### Declaration of competing interest

The authors declare that they have no known competing financial interests or personal relationships that could have appeared to influence the work reported in this paper.

#### Data availability

Data will be made available on request.

#### Appendix A. Noisy data

To account for possible random errors during measurements, noisy synthetic IV characteristics were also simulated. Then, the meta-heuristic algorithm was applied to extract the opposed two-diode model parameters, and the noise impact on the algorithm's effectiveness was evaluated.

In this case, the voltage  $V_i$  and the current  $I_i$  of each  $i$ th point of a IV characteristic were random values with a Gaussian distribution. The voltage mean value  $\bar{V}_i$  varied over a voltage range of 0–1.0 V with a 10 mV step; the current mean value  $\bar{I}_i$  was calculated using Eqs. (1)–(2),  $\bar{V}_i$ , and parameter values from Section 2.2.2 at  $T = 300$  K. The voltage standard deviation ( $SD_V$ ) was up to 0.1 mV, and the current standard deviation ( $SD_I$ ) was up to 1  $\mu$ A. Since the current in the IV curves varied from −1 mA to 1 mA and the voltage up to 1 V (see Fig. 3), the selected standard deviation values are entirely consistent with the measurement capabilities of modern instruments, such as the Keithley 2450 source meter. Thus, the different noisy IV curves were characterized by different  $SD_V$  and  $SD_I$  values; the idealized characteristic was defined by  $SD_V = 0$  V and  $SD_I = 0$  A.

When applying STLBO and ADELI to a single noisy IV curve, remarkably close parameter values were obtained. We used the absolute percentage error of the median value APE<sub>MEDIAN</sub> (see Eq. (10)) to quantify the error in parameter evaluation. Fig. 13 illustrates the increase in  $I_{01}$  and  $I_{02}$  extraction error by STLBO use with the rise in measurement error (standard deviation values increase). It should be noted that the presented error results are averaged for 100 IV curves simulated with the same standard deviation values for voltage and current. As the characteristics are generated using a random process, these 100 curves are distinct, resulting in varying parameter estimation error values. Additional materials include figure S23, which illustrates the corresponding dependencies for all eight model parameters.

For the idealized characteristic, the APE<sub>MEDIAN</sub> value ranged from  $1.3 \cdot 10^{-4}\%$  (for  $I_{02}$ ) to  $5.6 \cdot 10^{-2}\%$  (for  $R_{p1}$ ). As anticipated, the accuracy of parameter determination decreases for noisy IV curves. At the most intense noise level, the errors in determining  $I_{01}$  and  $R_s$  do not exceed 29%, while for  $R_{p1}$ , it is 26%. These parameters are extracted with the lowest accuracy. For  $I_{ph}$ ,  $I_{02}$ , and  $R_{p2}$ , the percentage error does not exceed 1%, which is an excellent result. The error in determining  $n_1$  is slightly higher at 2%.  $n_1$  demonstrates moderate accuracy, with an error rate of around 8%. Overall, STLBO and ADELI demonstrate resilience to measurement errors.

## Appendix B. Supplementary materials

Supplementary data to this article can be found online at <http://surl.li/udqju>.

## References

- [1] M. Zhang, W. Zhang, F. Zhang, C.-S. Lee, Y. Tang, Anion-hosting cathodes for current and late-stage dual-ion batteries, *Sci. China Chem.* 67 (5) (2024) 1485–1509.
- [2] M. Wang, C. Jiang, S. Zhang, X. Song, Y. Tang, H.-M. Cheng, Reversible calcium alloying enables a practical room-temperature rechargeable calcium-ion battery with a high discharge voltage, *Nature Chem.* 10 (6) (2018) 667–672.
- [3] X. Zhang, Y. Tang, F. Zhang, C.-S. Lee, A novel aluminum-graphite dual-ion battery, *Adv. Energy Mater.* 6 (11) (2016) 1502588.
- [4] X. Wang, X. Tian, X. Chen, L. Ren, C. Geng, A review of end-of-life crystalline silicon solar photovoltaic panel recycling technology, *Sol. Energy Mater. Sol.* 248 (2022) 111976.
- [5] D.H. Muhsen, A.B. Ghazali, T. Khatib, I.A. Abed, A comparative study of evolutionary algorithms and adapting control parameters for estimating the parameters of a single-diode photovoltaic module's model, *Renew. Energ.* 96 (2016) 377–389.
- [6] R. Abbassi, A. Abbassi, A.A. Heidari, S. Mirjalili, An efficient salp swarm-inspired algorithm for parameters identification of photovoltaic cell models, *Energy Convers. Manage.* 179 (2019) 362–372.
- [7] T. Sudhakar Babu, J. Prasanth Ram, K. Sangeetha, A. Laudani, N. Rajasekar, Parameter extraction of two diode solar PV model using Fireworks algorithm, *Sol. Energy* 140 (2016) 265–276.
- [8] H.M. Ridha, H. Hizam, C. Gomes, A.A. Heidari, H. Chen, M. Ahmadipour, D.H. Muhsen, M. Alghrairi, Parameters extraction of three diode photovoltaic models using boosted LSHADE algorithm and Newton raphson method, *Energy* 224 (2021) 120136.
- [9] A. Rezaee Jordehi, Enhanced leader particle swarm optimisation (ELPSO): An efficient algorithm for parameter estimation of photovoltaic (PV) cells and modules, *Sol. Energy* 159 (2018) 78–87.
- [10] N. Barth, R. Jovanovic, S. Ahzi, M.A. Khaleel, PV panel single and double diode models: Optimization of the parameters and temperature dependence, *Sol. Energy Mater. Sol.* 148 (2016) 87–98.
- [11] J.P. Ram, T.S. Babu, T. Dragicevic, N. Rajasekar, A new hybrid bee pollinator flower pollination algorithm for solar PV parameter estimation, *Energy Convers. Manage.* 135 (2017) 463–476.
- [12] H.M. Ridha, Parameters extraction of single and double diodes photovoltaic models using Marine Predators Algorithm and Lambert W function, *Sol. Energy* 209 (2020) 674–693.
- [13] M. Abdel-Basset, D. El-Shahat, R.K. Chakrabortty, M. Ryan, Parameter estimation of photovoltaic models using an improved marine predators algorithm, *Energy Convers. Manage.* 227 (2021) 113491.
- [14] H. Chen, S. Jiao, A.A. Heidari, M. Wang, X. Chen, X. Zhao, An opposition-based sine cosine approach with local search for parameter estimation of photovoltaic models, *Energy Convers. Manage.* 195 (2019) 927–942.
- [15] A.M. Beigi, A. Maroosi, Parameter identification for solar cells and module using a Hybrid Firefly and Pattern Search Algorithms, *Sol. Energy* 171 (2018) 435–446.
- [16] G. Xiong, J. Zhang, D. Shi, Y. He, Parameter extraction of solar photovoltaic models using an improved whale optimization algorithm, *Energy Convers. Manage.* 174 (2018) 388–405.
- [17] M. Abdel-Basset, R. Mohamed, S.A.A. Azeem, M. Jameel, M. Abouhawwash, Kepler optimization algorithm: A new metaheuristic algorithm inspired by Kepler's laws of planetary motion, *Knowl.-Based Syst.* 268 (2023) 110454.
- [18] S. Li, W. Gong, Q. Gu, A comprehensive survey on meta-heuristic algorithms for parameter extraction of photovoltaic models, *Renew. Sustain. Energy Rev.* 141 (2021) 110828.
- [19] B. Yang, J. Wang, X. Zhang, T. Yu, W. Yao, H. Shu, F. Zeng, L. Sun, Comprehensive overview of meta-heuristic algorithm applications on PV cell parameter identification, *Energy Convers. Manage.* 208 (2020) 112595.
- [20] D. Wolpert, W. Macready, No free lunch theorems for optimization, *IEEE Trans. Evol. Comput.* 1 (1) (1997) 67–82.
- [21] R. Saive, S-shaped current-Voltage characteristics in solar cells: A review, *IEEE J. Photovolt.* 9 (6) (2019) 1477–1484.
- [22] P.J. Roland, K.P. Bhandari, R.J. Ellington, Electronic circuit model for evaluating S-kink distorted current-voltage curves, in: 2016 IEEE 43rd Photovoltaic Specialists Conference, PVSC, 2016, pp. 3091–3094.
- [23] A. Gaur, P. Kumar, An improved circuit model for polymer solar cells, *Prog. Photovolt., Res. Appl.* 22 (9) (2014) 937–948.
- [24] V.-H. Tran, R.B. Ambade, S.B. Ambade, S.-H. Lee, I.-H. Lee, Low-temperature solution-processed SnO<sub>2</sub> nanoparticles as a cathode buffer layer for inverted organic solar cells, *ACS Appl. Mater. Interfaces* 9 (2) (2017) 1645–1653.
- [25] G. Lastra, V.S. Balderrama, L. Reséndiz, J. Pallarès, L.F. Marsal, V. Cabrera, M. Estrada, Air environment degradation of a high-performance inverted PTB7-Th:PC70BM solar cell, *IEEE J. Photovolt.* 9 (2) (2019) 464–468.
- [26] F. Xu, J. Zhu, R. Cao, S. Ge, W. Wang, H. Xu, R. Xu, Y. Wu, M. Gao, Z. Ma, F. Hong, Z. Jiang, Elucidating the evolution of the current-voltage characteristics of planar organometal halide perovskite solar cells to an S-shape at low temperature, *Sol. Energy Mater. Sol.* 157 (2016) 981–988.
- [27] J. Gao, J.M. Luther, O.E. Semonin, R.J. Ellington, A.J. Nozik, M.C. Beard, Quantum dot size dependent J-V characteristics in heterojunction ZnO/PbS quantum dot solar cells, *Nano Lett.* 11 (3) (2011) 1002–1008.
- [28] F. Yu, G. Huang, W. Lin, C. Xu, W. Deng, X. Ma, J. Huang, Lumped-parameter equivalent circuit modeling of solar cells with S-shaped I-V characteristics, *Solid-State Electron.* 156 (2019) 79–86.
- [29] E. Veinberg-Vidal, C. Dupré, P. García-Linares, C. Jany, R. Thibon, T. Card, T. Salvetat, P. Scheiblin, C. Brughera, F. Fournel, Y. Desieres, Y. Veschetto, V. Sanzone, P. Mur, J. Decobert, A. Datas, Manufacturing and characterization of III–IV on silicon multijunction solar cells, *Energy Procedia* 92 (2016) 242–247.
- [30] B. Romero, G. del Pozo, B. Arredondo, D. Martín-Martín, M.P.R. Gordoa, A. Pickering, A. Pérez-Rodríguez, E. Barrena, F.J. García-Sánchez, S-shaped I – V characteristics of organic solar cells: Solving Mazhari's lumped-parameter equivalent circuit model, *IEEE Trans. Electron Devices* 64 (11) (2017) 4622–4627.
- [31] B.Y. Finck, B.J. Schwartz, Understanding the origin of the S-curve in conjugated polymer/fullerene photovoltaics from drift-diffusion simulations, *Appl. Phys. Lett.* 103 (5) (2013) 053306.
- [32] D.S. Pillai, B. Sahoo, J.P. Ram, A. Laudani, N. Rajasekar, N. Sudhakar, Modelling of organic photovoltaic cells based on an improved reverse double diode model, *Energy Procedia* 117 (2017) 1054–1061.
- [33] B. Mazhari, An improved solar cell circuit model for organic solar cells, *Sol. Energy Mater. Sol.* 90 (7) (2006) 1021–1033.
- [34] F. Yu, G. Huang, W. Lin, C. Xu, An analysis for S-shaped I-V characteristics of organic solar cells using lumped-parameter equivalent circuit model, *Sol. Energy* 177 (2019) 229–240.
- [35] L. Zuo, J. Yao, H. Li, H. Chen, Assessing the origin of the S-shaped I-V curve in organic solar cells: An improved equivalent circuit model, *Sol. Energy Mater. Sol.* 122 (2014) 88–93.
- [36] F.A. de Castro, J. Heier, F.A. Nüesch, R. Hany, Origin of the kink in current-density versus voltage curves and efficiency enhancement of polymer-C<sub>60</sub> heterojunction solar cells, *IEEE J. Sel. Top. Quantum Electron.* 16 (6) (2010) 1690–1699.
- [37] F.J. García-Sánchez, D. Lugo-Muñoz, J. Muci, A. Ortiz-Conde, Lumped parameter modeling of organic solar cells' S-shaped I-V characteristics, *IEEE J. Photovolt.* 3 (1) (2013) 330–335.
- [38] F. De Castro, A. Laudani, F. Riganti Fulgini, A. Salvini, An in-depth analysis of the modelling of organic solar cells using multiple-diode circuits, *Sol. Energy* 135 (2016) 590–597.
- [39] E. Sesa, D. Darwisi, X. Zhou, W.J. Belcher, P.C. Dastoor, Experimental determination of the relationship between the elements of a back-to-back diode model for organic photovoltaic cells' S-shaped I-V characteristics and cell structure, *AIP Adv.* 9 (2) (2019) 025014.
- [40] F.J. García-Sánchez, B. Romero, Equivalent circuit models for next generation photovoltaic devices with S-shaped I-V curves, in: 2019 8th International Symposium on Next Generation Electronics, ISNE, 2019, pp. 1–4.
- [41] F.J. García-Sánchez, B. Romero, D. Lugo-Muñoz, G. del Pozo, B. Arredondo, J.J. Liou, A. Ortiz-Conde, Modelling solar cell S-shaped IV characteristics with DC lumped-parameter equivalent circuit - A review, *Facta Univ. Ser. Electron. Energetics* 30 (2017) 327–350.
- [42] J. Dakin, R. Brown (Eds.), *Handbook of Optoelectronics: Enabling Technologies* (Volume Two), second ed., CRC Press, 2017.
- [43] B. Arredondo, B. Romero, M. Beliatis, G. del Pozo, D. Martín-Martín, J. Blakesley, G. Dibb, F. Krebs, S. Gevorgyan, F. Castro, Analysing impact of oxygen and water exposure on roll-coated organic solar cell performance using impedance spectroscopy, *Sol. Energy Mater. Sol.* 176 (2018) 397–404.
- [44] G. del Pozo, B. Romero, B. Arredondo, Evolution with annealing of solar cell parameters modeling the S-shape of the current-voltage characteristic, *Sol. Energy Mater. Sol.* 104 (2012) 81–86.
- [45] D. Brenes-Badilla, D.J. Coutinho, D.R.B. Amorim, R.M. Faria, M.C. Salvadori, Reversing an S-kink effect caused by interface degradation in organic solar cells through gold ion implantation in the PEDOT:PSS layer, *J. Appl. Phys.* 123 (15) (2018) 155502.
- [46] K. Tada, Parameter extraction from S-shaped current-voltage characteristics in organic photocell with opposed two-diode model: Effects of ideality factors and series resistance, *Phys. Status Solidi A* 212 (8) (2015) 1731–1734.
- [47] M. Makha, P. Schwaller, K. Strassel, S.B. Anantharaman, F. Nüesch, R. Hany, J. Heier, Insights into photovoltaic properties of ternary organic solar cells from phase diagrams, *Sci. Technol. Adv. Mater.* 19 (1) (2018) 669–682.
- [48] G. Verkhogliadov, A. Mahmoodpoor, P. Voroshilov, R. Haroldson, M. Alahbakhshi, A.G. Nasibulin, S.V. Makarov, A.A. Zakhidov, Photoinduced self-gating of perovskite photovoltaic cells in ionic liquid, *ACS Mater. Au* 3 (4) (2023) 337–350.
- [49] A. Mahmoodpoor, G. Verkhogliadov, R. Melnikov, D.S. Saranin, P.M. Voroshilov, D. Sapori, R. Haroldson, A.G. Nasibulin, A.R. Ishteev, V. Ulyantsev, S.V. Makarov, A.A. Zakhidov, Ionic liquid gating in perovskite solar cells with fullerene/carbon nanotube collectors, *Energy Technol.* 10 (9) (2022) 2200485.

- [50] B. Romero, G. del Pozo, B. Arredondo, Exact analytical solution of a two diode circuit model for organic solar cells showing S-shape using Lambert W-functions, *Sol. Energy* 86 (10) (2012) 3026–3029.
- [51] K. Roberts, S.R. Valluri, On calculating the current-voltage characteristic of multi-diode models for organic solar cells, 2015, p. 1601.02679,
- [52] L. Lózzi, Guaranteed- and high-precision evaluation of the Lambert W function, *Appl. Math. Comput.* 433 (2022) 127406.
- [53] K. Tada, Bayesian estimation of equivalent circuit parameters of photovoltaic cell with S-shaped current-Voltage characteristic, *Phys. Status Solidi A* 218 (24) (2021) 2100403.
- [54] S.M. Sze, M. Lee, *Semiconductor Devices: Physics and Technology*, third ed., John Wiley & Sons, Inc, New York, 2012.
- [55] S. Kondratenko, V. Lysenko, Y.V. Gomeniuk, O. Kondratenko, Y. Kozyrev, O. Selyshchev, V. Dzhagan, D.R.T. Zahn, Charge carrier transport, trapping, and recombination in PEDOT:PSS/n-Si solar cells, *ACS Appl. Energy Mater.* 2 (8) (2019) 5983–5991.
- [56] M.A. Green, General temperature dependence of solar cell performance and implications for device modelling, *Prog. Photovolt., Res. Appl.* 11 (5) (2003) 333–340.
- [57] R. Eberle, A. Fell, F. Schindler, J. Shahid, M.C. Schubert, Breakdown of temperature sensitivity of silicon solar cells by simulation input parameters, *Sol. Energy Mater. Sol.* 219 (2021) 110836.
- [58] H. Ibrahim, N. Anani, Variations of PV module parameters with irradiance and temperature, *Energy Procedia* 134 (2017) 276–285.
- [59] F. Bradascia, M.C. Cavalcanti, A.J. do Nascimento, E.A. da Silva, G.M. de Souza Azevedo, Parameter identification for PV modules based on an environment-dependent double-diode model, *IEEE J. Photovolt.* 9 (5) (2019) 1388–1397.
- [60] A.H. Tuan Le, R. Basnet, D. Yan, W. Chen, N. Nandakumar, S. Duttagupta, J.P. Seif, Z. Hameiri, Temperature-dependent performance of silicon solar cells with polysilicon passivating contacts, *Sol. Energy Mater. Sol.* 225 (2021) 111020.
- [61] O. Dupré, R. Vaillon, M.A. Green, Experimental assessment of temperature coefficient theories for silicon solar cells, *IEEE J. Photovolt.* 6 (1) (2016) 56–60.
- [62] Y. Riesen, M. Stuckelberger, F.-J. Haug, C. Ballif, N. Wyrtsch, Temperature dependence of hydrogenated amorphous silicon solar cell performances, *J. Appl. Phys.* 119 (4) (2016) 044505.
- [63] A. Rana, A. Kumar, S. Chand, R.K. Singh, Exploring deep defect state impact on open circuit voltage of conventional and inverted organic solar cells, *J. Appl. Phys.* 124 (10) (2018) 103101.
- [64] M. Braik, A. Hammouri, J. Atwan, M.A. Al-Betar, M.A. Awadallah, White shark optimizer: A novel bio-inspired meta-heuristic algorithm for global optimization problems, *Knowl.-Based Syst.* 243 (2022) 108457.
- [65] J.-S. Pan, L.-G. Zhang, R.-B. Wang, V. Snášel, S.-C. Chu, Gannet optimization algorithm : A new metaheuristic algorithm for solving engineering optimization problems, *Math. Comput. Simulation* 202 (2022) 343–373.
- [66] S. Zhao, T. Zhang, S. Ma, M. Chen, Dandelion optimizer: A nature-inspired metaheuristic algorithm for engineering applications, *Eng. Appl. Artif. Intell.* 114 (2022) 105075.
- [67] K. Wang, M. Ye, Parameter determination of Schottky-barrier diode model using differential evolution, *Solid-State Electron.* 53 (2) (2009) 234–240.
- [68] K. Ishaque, Z. Salam, H. Taheri, A. Shamsudin, A critical evaluation of EA computational methods for Photovoltaic cell parameter extraction based on two diode model, *Sol. Energy* 85 (9) (2011) 1768–1779.
- [69] Q. Huang, K. Zhang, J. Song, Y. Zhang, J. Shi, Adaptive differential evolution with a Lagrange interpolation argument algorithm, *Inform. Sci.* 472 (2019) 180–202.
- [70] M. Tian, X. Gao, Differential evolution with neighborhood-based adaptive evolution mechanism for numerical optimization, *Inform. Sci.* 478 (2019) 422–448.
- [71] R. Tanabe, A.S. Fukunaga, Improving the search performance of SHADE using linear population size reduction, in: 2014 IEEE Congress on Evolutionary Computation, CEC, 2014, pp. 1658–1665.
- [72] A.W. Mohamed, A.A. Hadi, K.M. Jambi, Novel mutation strategy for enhancing SHADE and LSHADE algorithms for global numerical optimization, *Swarm Evol. Comput.* 50 (2019) 100455.
- [73] M. Ye, X. Wang, Y. Xu, Parameter extraction of solar cells using particle swarm optimization, *J. Appl. Phys.* 105 (9) (2009) 094502.
- [74] N. Karaboga, S. Kockanat, H. Dogan, The parameter extraction of the thermally annealed schottky barrier diode using the modified artificial bee colony, *Appl. Intell.* 38 (3) (2013) 279–288.
- [75] S. Mirjalili, A. Lewis, The whale optimization algorithm, *Adv. Eng. Softw.* 95 (2016) 51–67.
- [76] D. Oliva, M. Abd El Aziz, A. Ella Hassanien, Parameter estimation of photovoltaic cells using an improved chaotic whale optimization algorithm, *Appl. Energy* 200 (2017) 141–154.
- [77] A. Sadollah, H. Sayyaadi, A. Yadav, A dynamic metaheuristic optimization model inspired by biological nervous systems: Neural network algorithm, *Appl. Soft Comput.* 71 (2018) 747–782.
- [78] S.J. Patel, A.K. Panchal, V. Kheraj, Extraction of solar cell parameters from a single current-voltage characteristic using teaching learning based optimization algorithm, *Appl. Energy* 119 (2014) 384–393.
- [79] X. Chen, K. Yu, W. Du, W. Zhao, G. Liu, Parameters identification of solar cell models using generalized oppositional teaching learning based optimization, *Energy* 99 (2016) 170–180.
- [80] Q. Niu, H. Zhang, K. Li, An improved TLBO with elite strategy for parameters identification of PEM fuel cell and solar cell models, *Int. J. Hydrogen Energy* 39 (8) (2014) 3837–3854.
- [81] R.M. May, Simple mathematical models with very complicated dynamics, *Nature* 261 (5560) (1976) 459–467.
- [82] Y.-J. Zheng, Water wave optimization: A new nature-inspired metaheuristic, *Comput. Oper. Res.* 55 (2015) 1–11.
- [83] R. Rao, Jaya: A simple and new optimization algorithm for solving constrained and unconstrained optimization problems, *Int. J. Ind. Eng. Comput.* 7 (2016) 19–34.
- [84] K. Yu, J. Liang, B. Qu, X. Chen, H. Wang, Parameters identification of photovoltaic models using an improved JAYA optimization algorithm, *Energy Convers. Manage.* 150 (2017) 742–753.
- [85] S. Mirjalili, SCA: A Sine cosine algorithm for solving optimization problems, *Knowl.-Based Syst.* 96 (2016) 120–133.
- [86] W. Long, T. Wu, X. Liang, S. Xu, Solving high-dimensional global optimization problems using an improved sine cosine algorithm, *Expert Syst. Appl.* 123 (2019) 108–126.
- [87] S. Gupta, K. Deep, A hybrid self-adaptive sine cosine algorithm with opposition based learning, *Expert Syst. Appl.* 119 (2019) 210–230.
- [88] P.P. Biswas, P. Suganthan, G. Wu, G.A. Amaralunga, Parameter estimation of solar cells using datasheet information with the application of an adaptive differential evolution algorithm, *Renew. Energ.* 132 (2019) 425–438.
- [89] J. Derrac, S. García, D. Molina, F. Herrera, A practical tutorial on the use of nonparametric statistical tests as a methodology for comparing evolutionary and swarm intelligence algorithms, *Swarm Evol. Comput.* 1 (1) (2011) 3–18.
- [90] V. Sahargahi, V. Majidnezhad, S.T. Afshord, Y. Jafari, An intelligent chaotic clonal optimizer, *Appl. Soft Comput.* 115 (2022) 108126.
- [91] J. Zhu, R. Chaturvedi, Y. Fouad, I. Albaijan, N. Juraev, L.H. Alzubaidi, I. Mahariq, A. Afandi, H.A. Garalleh, A numerical modeling of battery thermal management system using nano-enhanced phase change material in hot climate conditions, *Case Stud. Therm. Eng.* 58 (2024) 104372.
- [92] C. Zhu, Optimizing and using AI to study of the cross-section of finned tubes for nanofluid-conveying in solar panel cooling with phase change materials, *Eng. Anal. Bound. Elem.* 157 (2023) 71–81.
- [93] V.J. Chin, Z. Salam, A new three-point-based approach for the parameter extraction of photovoltaic cells, *Appl. Energy* 237 (2019) 519–533.
- [94] V.J. Chin, Z. Salam, K. Ishaque, An accurate and fast computational algorithm for the two-diode model of PV module based on a hybrid method, *IEEE Trans. Ind. Electron.* 64 (8) (2017) 6212–6222.
- [95] A. Ortiz-Conde, F.J. García Sánchez, J. Muci, New method to extract the model parameters of solar cells from the explicit analytic solutions of their illuminated I-V characteristics, *Sol. Energy Mater. Sol.* 90 (3) (2006) 352–361.